iScience

Article

Insulin acts on astrocytes to shift their substrate preference to fatty acids

Graphical abstract

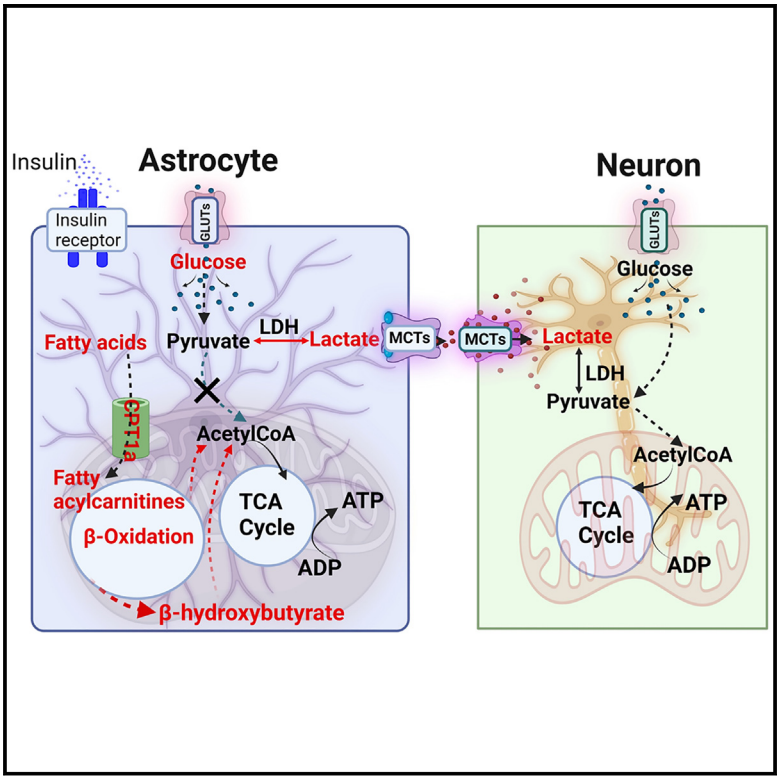

Highlights

- Insulin acts on astrocytes to shift their substrate preference to fatty acids
- Fatty acids are β-oxidized in sufficient quantity to satisfy astrocyte energy demands
- Pyruvate derived from glucose is directed away from the TCA cycle to form lactate
- LTP evoked by insulin requires fatty acid metabolism in astrocytes

Authors

Bouchra Taib, Pragney Deme, Sujasha Gupta, ..., Zhigang Li, Rexford S. Ahima, Norman J. Haughey

Correspondence

nhaughey@tulane.edu

In brief

Natural sciences; Biological sciences; Neuroscience; Systems neuroscience; Cellular neuroscience.

Taib et al., 2025, iScience *28*, 111642
April 18, 2025
https://doi.org/10.1016/j.isci.2024.111642

CellPress

iScience

CellPress
OPEN ACCESS

Article

Insulin acts on astrocytes to shift their substrate preference to fatty acids

Bouchra Taib,[1,5,7] Pragney Deme,[2,7,8] Sujasha Gupta,[2] Seung Wan Yoo,[2] Saja S. Khuder,[2] Ahmet Hoke,[2,4] Zhigang Li,[2] Rexford S. Ahima,[1] and Norman J. Haughey[2,3,6,8,9,*]

[1]The Johns Hopkins University School of Medicine, Department of Medicine, Division of Endocrinology, Diabetes and Metabolism, Baltimore, MD, USA
[2]The Johns Hopkins University School of Medicine, Department of Neurology, Baltimore, MD, USA
[3]The Johns Hopkins University School of Medicine, Department of Psychiatry, Baltimore, MD, USA
[4]The Johns Hopkins University School of Medicine, Department of Neuromuscular Division, and Merkin Peripheral Neuropathy and Nerve Regeneration Center, Baltimore, MD, USA
[5]Institute of Sport Professions (IMS), Ibn Tofail University, Kenitra, Morocco
[6]Tulane University School of Medicine, New Orleans, LA, USA
[7]These authors contributed equally
[8]Senior author
[9]Lead contact
*Correspondence: nhaughey@tulane.edu
https://doi.org/10.1016/j.isci.2024.111642

SUMMARY

It is increasingly recognized that brain can β-oxidize fatty acids for use as an energy substrate. However, mechanism(s) by which neural cells switch their preference from glucose to fatty acids are not fully elucidated. Here we provide evidence that insulin acts directly on astrocytes to promote the uptake of glucose and fatty acids while modifying their substrate preference through a sequential shift in the expression of genes associated with fatty acid uptake, synthesis, transport, and metabolism. Under these conditions, fatty acids are converted into TCA cycle intermediates to satisfy astrocyte energy demands, allowing pyruvate derived from glucose to be directed toward the production of lactate; a preferred fuel for neurons. This shift in astrocyte energy substrate preference is required for insulin to enhance long-term potentiation in the Schaffer collateral. These findings establish a homeostatic mechanism where insulin promotes LTP by switching the energy substrate preference of astrocytes to fatty acids.

INTRODUCTION

Glucose and fatty acids are the primary energy substrates in mammals.[1] The dysregulation of glucose and/or fatty acid metabolism results in metabolic defects including obesity and diabetes[2] that can severely impact neurological function.[1,3] Although the brain relies mainly on glucose as an energy substrate,[4] there is increasing evidence that astrocytes are capable of oxidizing fatty acids under conditions of stress.[5–8] This response to stress appears to be protective, as evidenced by a recent report showing that hyperactive neurons circumvent the accumulation of toxic fatty acids by transferring them to astrocytes for β-oxidation.[5] Other reports have described neurotoxic roles for fatty acid oxidation in astrocytes.[9,10] In addition to these stress-triggered metabolic adaptations, it is still a matter of debate if the oxidation of fatty acids by astrocytes is part of a homeostatic mechanism regulating brain energy homeostasis.[7,11,12]

Insulin is a master regulator of energy metabolism. In peripheral tissues, insulin promotes cellular glucose uptake, stimulates glycolysis, and inhibits lipolysis.[13] In the brain, the roles of insulin in regulating energy metabolism are not well understood. Insulin receptors are widely distributed throughout the brain with the highest concentrations in the olfactory bulb, followed by the cerebral cortex, hippocampus, hypothalamus, thalamus, and cerebellum.[14–16] Insulin is thought to enter into the brain from peripheral circulation via a saturable transport system[17] and can readily access regions of the brain such as the basal hypothalamus where the blood-brain barrier is less stringent or may be altogether absent. The known central actions of insulin are involved with the regulation of body weight and food intake, cognitive processes and memory function.[18,19] Impairments of insulin signaling have been associated with neurodegenerative conditions.[20] For example, individuals with type 1 or type 2 diabetes exhibit age-related declines in cognition, are more likely to develop Alzheimer's disease (AD), and show a faster trajectory of cognitive decline compared with patients with non-diabetic AD.[21–23]

The brain contains numerous types of fatty acids including saturated, monounsaturated, and long-chain polyunsaturated fatty acids (PUFAs)[24] that is expressed in glia and neurons.[25] The vast majority of studies have focused on PUFA metabolism in the brain with an emphasis on the regulation of neuronal survival, neurogenesis, synaptic function and brain inflammation.[26,27] Although fatty acid metabolism has been extensively studied in the peripheral organs,[28–30] roles for fatty acids as

energy substrates in the brain remains controversial.[31,32] While glucose is the primary energy substrate for the brain,[4] under some conditions lactate[33] and ketones[34,35] can substitute as the main substrates for energy metabolism. As neurons are less capable of storing lipids in droplets, or utilizing glycogen as an energy reserve, the energy substrates available in neurons deplete rapidly under conditions of high activity.[33] In contrast to neurons, astrocytes have considerable capacity to store glycogen[36] and lipids.[37] It is widely believed that metabolic coupling between astrocytes and neurons plays a vital role in maintaining neuronal function during periods of high activity that include a lactate shuttle,[38] glutamate-glutamine shuttle,[39] lipid recycling,[40] and neuronal detoxification.[5] Here we provide experimental evidence that in response to insulin, astrocytes shift their metabolic preference to fatty acids. These fatty acids are converted into TCA cycle intermediates in sufficient quantity to satisfy astrocyte energy demands. Under these conditions, pyruvate derived from glucose is directed away from the TCA cycle to accelerate the production of lactate that is a preferred fuel for neurons. This metabolic switch in astrocytes is critical for insulin to promote LTP in the Schaffer collateral.

RESULTS

Intranasal insulin regulates pathways and functions involved with glucose and fatty acid metabolism in the hippocampus

To investigate the effects of insulin on brain energy metabolism, we administered insulin (INI; 1.2 IU/nare; 2.4 IU total) or saline intranasally into mice and sacrificed them after 15min, 1h or 6h. RNA sequencing (RNAseq) was performed on hippocampal tissues. A total of 46,202 transcripts were detected. Genes were filtered by setting the minimum Fragments Per Kilobase of transcript per Million (FPKM) value to log2 and differentially expressed genes were used to identify signaling pathways and functions modified by insulin. Within 15 min of INI administration, 181 transcripts were upregulated and 55 were downregulated (Figure 1B). At this early time point, genes with altered expression were almost exclusively related to neuronal functions; none of these genes were associated with energy metabolism. The identified pathways at 15 min post-INI were associated with dendritic cell maturation, ERK/MAPK, cAMP, TR/RXR activation, dopamine receptor activity, and Wnt/Ca^{+} signaling (Figure 1C). Functional associations were largely related to the neurotrophic functions of insulin, or cross-talk with insulin-associated signaling pathways that included cognition, neurotransmission, learning, dendritic growth/branching, synaptic transmission, memory, neuritogenesis, development of neurons, and organization of cytoskeleton (Figure S1B).

One hour following INI administration, 173 transcripts were upregulated and 140 were downregulated (Figure 1D**)**. At this timepoint, the expression of 12 genes associated with the metabolism of lipids and fatty acids was increased. The identified pathways at 1h post-INI were associated with ERK/MAPK, cAMP, TR/RXR signaling, oxidative phosphorylation, and AMPK signaling (Figure 1E). Functional associations at this time point were exclusively related to glucose and lipid metabolism including the secretion of lipids, the oxidation, the concentration of D-glucose, release of fatty acids, the release of lipids, and quantity of carbohydrates (Figure S1C).

Six hours following INI administration, 164 transcripts were elevated and 77 were downregulated (Figure 1F). At this late time point genes with elevated expression were largely associated with lipid metabolism and included RAR, PXR/RXR, and TR/RXR activation, AMPK, phosphatidylethalomine, phosphatidylcholine, retinoate biosynthesis, oxidative phosphorylation, and Wnt/Ca+ signaling (Figure 1G). Functional associations 6h post-INI were exclusively related to energy metabolism including insulin sensitivity, accumulation of lipids, glucose tolerance, the release of fatty acid and lipids (Figure S1D). These data demonstrate that insulin delivered to the brain by intranasal administration produces a rapid, robust, and time-dependent modification in gene expression with early effects that appear to be neurotrophic, with a slower downstream activation of energy pathways related to the metabolism of lipids. A complete list of genes modified in abundance at each experimental time point is available on GEO (GSE280416 and GSE280417). Genes with modified expression in the specified signaling pathways can be found in supplementary data (Tables S1A–S1C).

Insulin increases the expression of genes involved in sphingolipid, sterol, and fatty acid metabolism in astrocytes

We next sought to determine the effects of insulin on global gene expression in isolated primary astroglia. We detected a total of 37,185 transcripts in astroglial cultures. After a 6h exposure to insulin 883 transcripts were upregulated 2SD or greater and 852 transcripts were downregulated 2SD or greater compared with vehicle treated cultures (Figure 2B). Bioinformatic interrogation of genes with expression greater or less than 2SD at the 6h time point identified signaling pathways associated with fatty acid activation, cAMP, Wnt/Ca^{2+}, β-oxidation, ceramide biosynthesis/degradation, gap junction, dendritic cell maturation, triacylglycerol degradation and phospholipase activation (Figure 2C). Functions included the quantity of diacylglycerol, synthesis of sterols, cholesterol, and carbohydrates, synthesis of esterification of lipids, cholesterol metabolism, and adipogenesis (Figure S2B). After exposing cultured astrocytes to insulin for 12h, the expression of 811 genes was upregulated by 2SD or greater, and 849 genes were decreased by 2SD or greater compared with vehicle treated astrocytes (Figure 2D**)**. At this time point, bioinformatic analysis identified signaling pathways associated with fatty acid activation, fatty acid β-oxidation, stearate biosynthesis, glycolysis, CDP-diacylglycerol biosynthesis, pyruvate to lactate production, ceramide degradation, cAMP-mediated signaling, and triacylglycerol degradation (Figure 2E**)**. Functional associations were almost exclusively related to the synthesis and storage of sterols and lipids (Figure S2C). The signaling and functional classifications identified suggest that insulin promotes a robust metabolism of lipids in astrocytes. Genes with modified expression at each time point and associated signaling pathways can be found in supplementary data (Tables S2A and S2B). A complete list of genes can be found in GEO (*submitted and pending*).

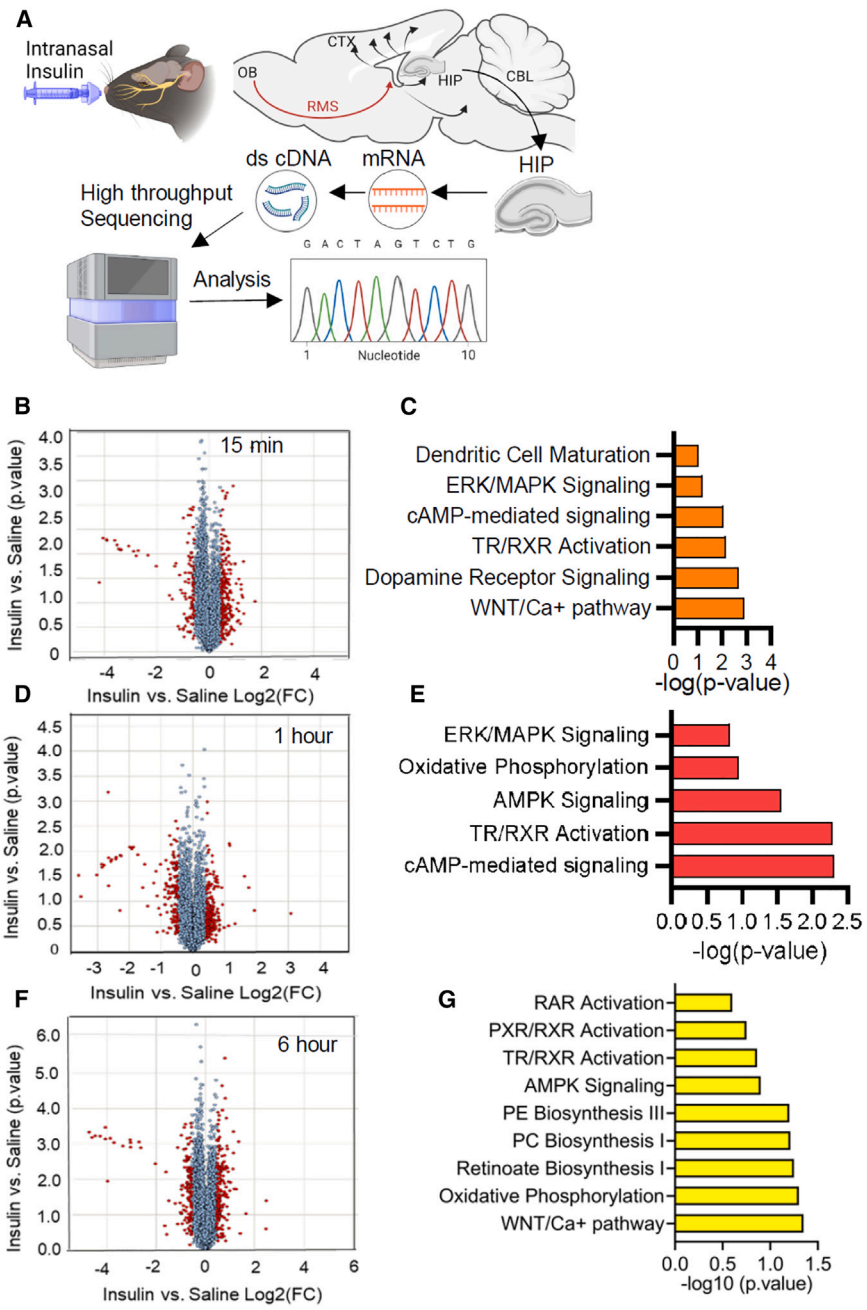

Figure 1. Intranasal insulin (INI) promoted a rapid upregulation of gene products associated with the neurotrophic effects of insulin, followed by an upregulation of gene products associated with lipid metabolism

(A) INI (1.2 IU/nare; 2.4 IU total) or saline was administered to mice and animals sacrificed after 15min, 1h and 6h. INI enters into brain through the cribriform plate and distributes rostrally throughout the brain. RNA sequencing was conducted using hippocampal tissues. Gene products increased or decreased 1.5-fold or greater by INI compared with saline were included for informatic analysis.

(B) Within 15 min of INI 181 transcripts were upregulated and 55 were downregulated.

(C) Primary signaling pathways identified by informatic interrogation of gene products modified in abundance by INI within 15min are shown.

(D) Within 1h of INI 173 genes were upregulated and 140 genes were downregulated.

(E) Primary signaling pathways identified by informatic interrogation of gene products modified by INI within 1h are shown.

(F) At the 6h timepoint following INI 164 genes were increased and 77 decreased in the insulin group compared with mice administered saline.

(G) Primary signaling pathways identified by informatic interrogation of gene products modified by INI at the 6h time point are shown. Data are from $n = 2$.

Insulin increases the expression of genes mediating trophic and protective responses in neurons

We next exposed primary neuronal cultures to insulin and conducted RNA sequencing. Exposing neurons to insulin for 6h resulted in the upregulation of 753 transcripts 2SD or greater and the downregulation of 660 transcripts 2SD or greater compared to vehicle treated cultures (Figure 2G**)**. Signaling pathways associated with insulin-modified gene expression included actin-based motility by Rho, Wnt/β-catenin, tight junctions, axonal guidance, dendritic cell maturation, sero-/melatonin biosynthesis, serotonin receptor, and CREB signaling (Figure 2H). Functional associations included synaptogenesis, serotonin degradation, glutathione-mediated detoxification, sirtuin signaling, IL-15, and CREB-associated neuronal activation (Figure S2E). Insulin-associated changes in neuronal gene expression remained robust for at least 12h with 768 transcripts upregulated and 736 transcripts downregulated at this time point (Figure 2I**)**. Bioinformatic analysis of insulin evoked transcriptional changes at 12h identified signaling pathways associated with synaptogenesis, dendritic cell maturation, actin-based motility by Rho, actin cytoskeletal signaling, axonal guidance, signaling by Rho GTPases, and CREB (Figure 2J). Associated functions included synaptogenesis, regulation of actin-based motility, cytoskeletal activation, STAT3, Reelin, IL-15, and Tec kinase activation (Figure S2F). None of the insulin associated changes in gene expression were related to lipid, sterol, or fatty acid metabolism. These data suggest that insulin promotes neuroprotective and neurotrophic effects in cultured neurons. Genes with modified expression at each time point and associated with the specified signaling pathways can be found in supplementary data (Tables S2C and S2D). A complete list of these genes can be found in GEO (*submitted and pending*).

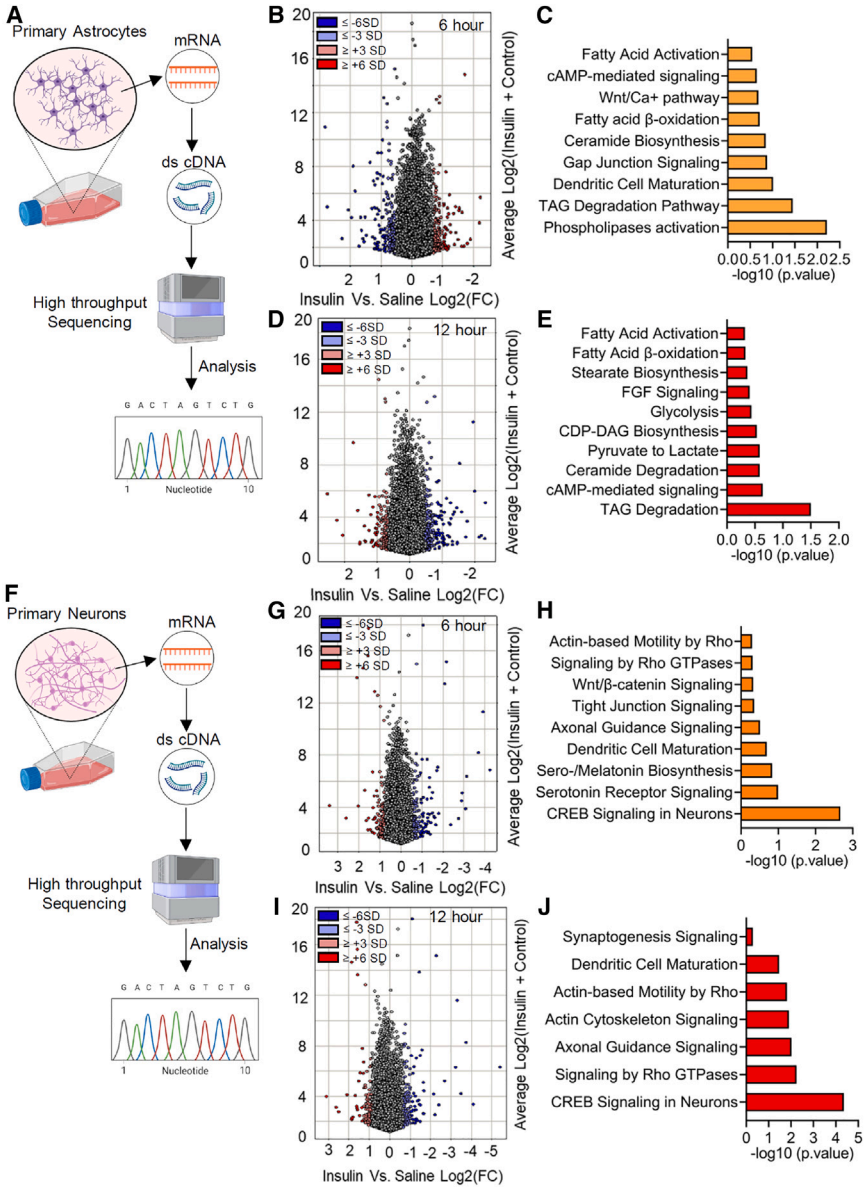

Figure 2. Insulin promotes substantially different patterns of gene expression in neurons and astrocytes

(A) Schematic representation of primary astrocyte cultures exposed to insulin (200 nM) for 6 or 12h and harvested for RNA sequencing. Gene products increased or decreased 1.5-fold or greater following insulin treatment compared with vehicle were included for informatic analysis.

(B) Exposing astrocytes to insulin for 6h resulted in the upregulation of 883 gene products and the downregulation of 852 gene products.

(C) Signaling pathways implicated by informatic interrogation of insulin-evoked changes in gene expression are shown.

(D) After exposing astrocytes to insulin for 12h, 811 gene products were upregulated, and 849 gene products downregulated.

(E) Signaling pathways implicated by informatic interrogation of insulin-evoked changes in gene expression are shown.

(F) Schematic representation of primary neuronal cultures exposed to insulin (200 nM) for 6 or 12h and harvested for RNA sequencing.

(G) In neurons following 6h of insulin exposure the expression of 753 gene products were upregulated and 660 gene products downregulated compared to vehicle exposed cultures.

(H) Signaling pathways implicated by informatic interrogation of insulin-evoked changes in gene expression are shown.

(I) After treating neurons for 12h with insulin the expression of 768 genes were upregulated and 736 genes downregulated.

(J) Signaling pathways implicated by informatic interrogation of insulin-evoked changes in gene expression are shown. Data are from $n = 2$.

Insulin promotes β-oxidation of fatty acids in astrocytes

We next focused our attention on the possibility that insulin promotes the β-oxidation of fatty acids in astrocytes for use as an energy substrate. We evaluated the effects of insulin on the expression of several genes involved in the regulation of sterol and fatty acid metabolism in astrocytes by RT-PCR. The treatment of primary astrocytes with insulin induced a rapid (1h) but transient increase in the expression of cytochrome *c* oxidase subunit II (COX-II; a mitochondrial encoded subunit of respiratory complex IV) and Pyruvate Dehydrogenase Kinase 4 (Pdk4; an insulin sensitive mitochondrial matrix protein) which inhibits activity of Pyruvate Dehydrogenase (PDH), which in turn will inhibit the conversion of pyruvate into Acetyl-CoA that diverts glucose from glycolysis to the TCA cycle and oxidative phosphorylation (Figures 3A and 3B). Insulin also rapidly increased the expression of Carnitine Palmitoyltransferase 1a (CPT1a; located in the outer mitochondria membrane and regulates the entry of fatty acids into mitochondria) for at least 12h (Figure 3C). After 6h of insulin exposure, we noted the increased expression of the fatty acid binding protein 7 (FABP7; binds long chain fatty acids to regulate fatty acid uptake, transport, and metabolism), short-chain acyl-CoA dehydrogenase (SCAD; located to mitochondria and catalyzes the first step of short-chain fatty acid β-oxidation), mitochondrial Trifunctional Protein Coenzyme A (MTP-CoA; located to the inner mitochondrial membrane and catalyzes the last 3 steps in β-oxidation), and fatty acid synthase (FASN; catalyzes the *de novo* synthesis of fatty acids) (Figures 3D–3G). FABP7 expression returned to levels not different from baseline within 12h, while MTP-CoA and SCAD expression remained elevated for at least 12h (Figures 3D–3F). After 12h of insulin exposure astrocytes upregulated the expression of mitochondrial uncoupling protein 3 (Ucp3; inner mitochondrial membrane protein that upregulates fatty acid metabolism[41]) and sterol regulatory binding element (Srebf1; an insulin responsive element coding for a group of

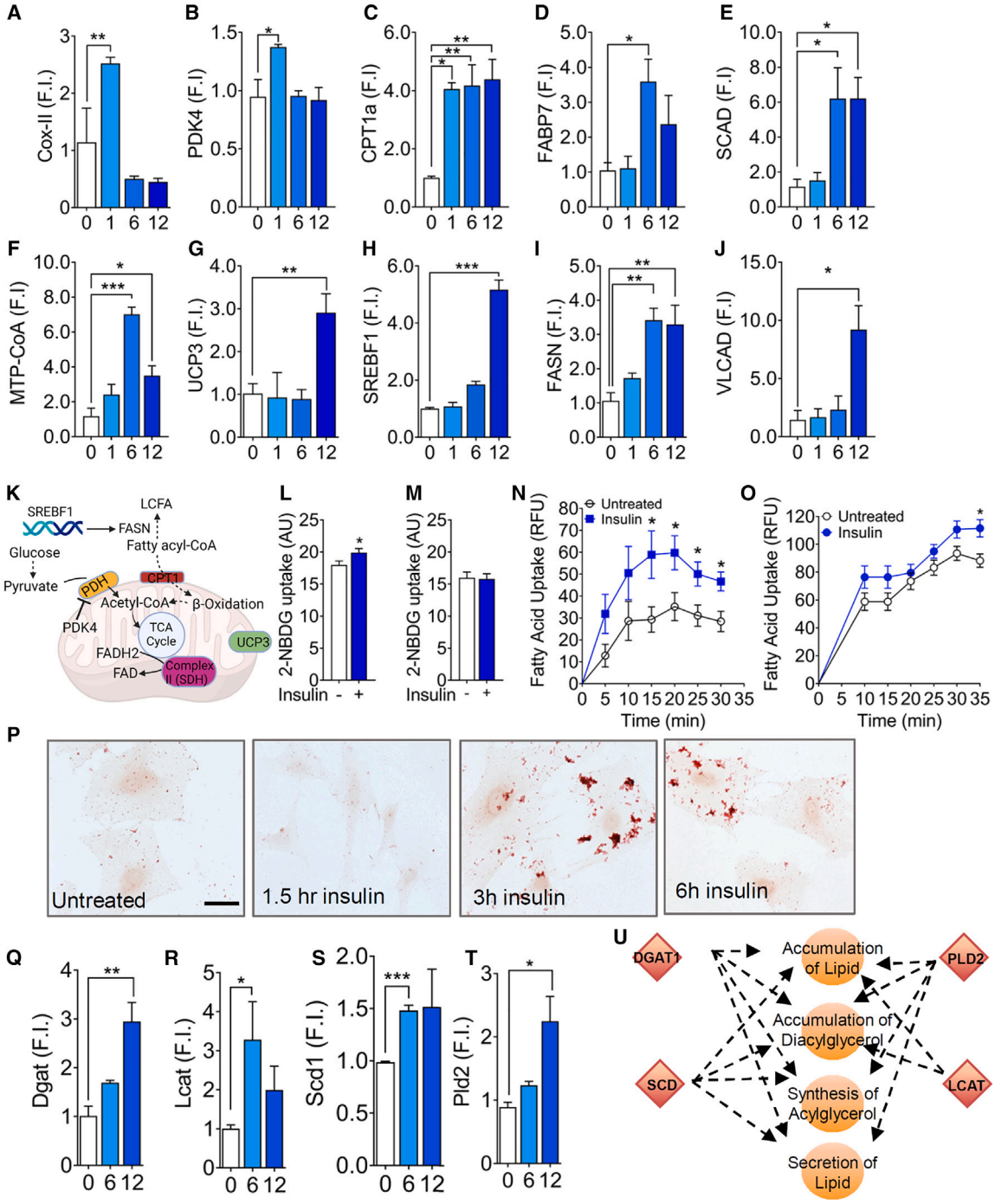

Figure 3. Astrocytes prepare to metabolize fatty acids following insulin exposure

(A–J) Primary cultured astrocytes were exposed to insulin (200 nM) and the expression of transcripts for proteins involved with sterol and fatty acid metabolism measured by qRT-PCR. The expression of mitochondrial genes (A) Cox-II (B) Pdk4, (C) CPT1a were increased within 1h of insulin exposure. Within 6h of insulin exposure genes regulating the biosynthesis of fatty acids, transport, and β-oxidation (D) FABP7, (E) SCAD, (F) MTP-CoA, and (G) FASN were increased. After 12h of insulin exposure (H) UCP3, (I) Srebf1, a gene regulating sterol biosynthesis and (J) VLCAD, a gene which facilitates the first step in the β-oxidation of very long chain fatty acids were increased.

(K) Depicts the location and function of the indicated gene products.

(L and M) The uptake of 2-NBG in (L) astrocytes and (M) neurons 30 min following the addition of insulin (200 nM) or vehicle.

(N and O) Fatty acid uptake was measured at 5min intervals for 30 min following the addition of insulin (200nM) in (N) astrocytes and (O) neurons.

(P) Oil Red O staining shows cellular accumulation of neutral lipids at the indicated time points following the insulin (200 nM) treatment of astrocytes.

(legend continued on next page)

transcription factors that regulate sterol biosynthesis), and very long-chain acyl-coenzyme A dehydrogenase (VLCAD; catalyzes the first steps of mitochondrial long chain fatty acid oxidation) (Figures 3H–3J). These data demonstrate that insulin promotes a timed expression of genes that increase the synthesis and mitochondrial uptake of fatty acids, followed by the expression of genes that prepare mitochondria to shift their substrate preference from glucose to fatty acids (Figure 3K).

Insulin increases fatty acid uptake in astrocytes

Consistent with published reports[42] we found that insulin increased glucose uptake in astrocytes[43] (Figure 3L) but had no effect on glucose uptake in neurons that are known to be insensitive to insulin[44] (Figure 3M). Insulin promoted a robust increase in the uptake of fatty acids in astrocytes that peaked between 15 and 20 min and was sustained for at least 30 min (Figure 3N). Although there was a time-dependent uptake of fatty acids into neurons, the rate of uptake was not increased by insulin (Figure 3O**)**. The insulin-evoked uptake of fatty acids in astrocytes was accompanied by a time-dependent accumulation of cytosolic neutral lipid droplets (Figure 3P) and the increased expression of genes associated with the synthesis and storage of neutral lipids including diglyceride acyltransferase (DGAT; catalyzes the formation of triglycerides from diacylglycerol and Acyl-CoA), lecithin–cholesterol acyltransferase (LCAT; regulates the conversion of free cholesterol into cholesteryl esters), stearoyl-CoA desaturase (SCD; catalyzes the rate-limiting step in the formation of monounsaturated fatty acids), and phospholipase D2 (PLD2; catalyzes the hydrolysis of PC to phosphatidic acid and choline to regulate the secretion of lipids) (Figures 3Q–3T). These data demonstrate that insulin increases the synthesis, storage, and secretion of neutral lipids in astrocytes (Figure 3U). Primers used for qRT-PCR are listed in Table S3.

Insulin promotes saturated free fatty acid utilization in astrocytes

We next examined the effects of insulin on metabolite profiles in astrocytes. Metabolites were filtered by setting the minimum fold change value > 1.5 and *raw p* value < 0.05. Within 3h of insulin exposure, 14 metabolites were increased and 5 were decreased (Figure 4A). Metabolites increased within 3h of insulin included fatty acids (n = 4), fatty acylcarnitines (n = 3), glucose, lactate, β-hydroxybutyrate (a ketone body), lysophosphocholines (LPC; n = 3) and lysophosphoethanolamines (LPE; n = 1). Metabolites decreased in abundance included α-Ketoisokaproate, LysoPEs (n = 3) and LysoPC (n = 1) (Figure 4B). At the 6h time point following insulin 17 metabolites were increased, and 3 metabolites decreased (Figure 4C). Increased metabolites included fatty acids (n = 5), fatty acylcarnitines (n = 5), lactate, TCA cycle intermediates (n = 2), β-hydroxybutyrate, LysoPCs (n = 1) and LysoPEs (n = 1). Decreased metabolites included LysoPCs (n = 2) and azelaic acid (Figure 4D). Following 12h of insulin exposure 17 metabolites were increased and 3 metabolites were decreased (Figure 4E). Increased metabolites included the amino acids tyrosine, glutathione, and glutamate, fatty acids (n = 4), fatty acylcarnitines (n = 1), carnitine, β-hydroxybutyrate, LysoPCs (n = 2), LysoPEs (n = 2), and lactate. Decreased metabolites included aconitate, Glycerophosphocholine, and azelaic acid (Figure 4F). These findings demonstrate that insulin increases the content of free fatty acids and glucose in astrocytes. The forms of fatty acids modified in abundance following insulin exposure suggests that the bulk of these fatty acids were modified for use as an energy substrate, as evidenced by elevated levels of fatty acylcarnitines, increased TCA cycle intermediates, and β-hydroxybutyrate, with a smaller component that may be targeted for glycerophsopholipid biosynthesis, presumably for membrane remodeling.

To further evaluate the use of fatty acids as an energy substrate we conducted a targeted analysis of fatty acids, acylcarnitines, and TCA cycle intermediates in cultured astrocytes exposed to insulin. Within 3-6h insulin promoted an increase of several saturated fatty acids including octanoic acid, decanoic acid, and myristic acid. Consistent with the requirement of fatty acids to be primed by Acetyl-Co-A synthase and conjugated to carnitine by CPT1 for transport across the mitochondrial membrane, we found that insulin increased the fatty acylcarnitine derivatives propionylcarnitine, myristoylcarnitine and palmitoylcarnitine (Figures 4G and 4H). We also found that insulin increased levels of β-hydroxy butyrate levels within 3-6h following insulin exposure, consistent with the β-oxidation of fatty acids to generate ketone bodies (Figure 4I). Levels of fatty acids, fatty acylcarnitines, and ketone bodies were not different from control levels within 12h of insulin exposure, suggesting that the fatty acids initially mobilized by insulin were subsequently metabolized.

In contrast to the impact of insulin on energy substrate shifting in astrocytes, metabolites upregulated in neurons exposed to insulin included the organic acids lactate, and stearate (associated with energy metabolism and neuronal protection),[45] amino-organic compounds (associated with neurotransmitter metabolism),[46] nudifloramide (a product of nicotinamide adenine dinucleotide metabolism)[47] and several saturated lipids including PC 14:0, 16:0, 16:1, 18:1; PE 14:1, 16:0 and MAG 18:1 (involved in the remodeling of cellular membranes and membrane trafficking)[48] (Figures S3A–S3F). Insulin had no effect on neuronal levels of fatty acids, fatty acylcarnitines, or ketone bodies at any time point tested (Figures S3G–S3I). A complete list of metabolites modified by insulin in astrocytes and neurons can be found in Tables S4 and S5 respectively.

Insulin regulation of glucose and fatty acid oxidation in mice with an astrocyte specific deletion of the insulin receptor

We confirmed our *in vitro* findings by administering INI to mice with an astrocyte specific deletion of the insulin receptor

(Q–T) The expression genes regulating the cellular handling of lipids (Q) Diglyceride acyltransferase (DGAT), (R) Lecithin–cholesterol acyltransferase (LCAT), (S) Stearoyl-CoA desaturase (SCD), and (T) phospholipase D2 (PLD2) were increased at the indicated time points following the insulin treatment of astrocytes. (U) A diagrammatic representation of lipid metabolism regulated by the indicated gene products. Data are mean ± SEM of n = 3–5 experiments per condition. * = $p < 0.05$, ** = $p < 0.01$ and ### = $p < 0.001$. ANOVA with Tukey post-hoc comparisons. Scale bar, 50 μm.

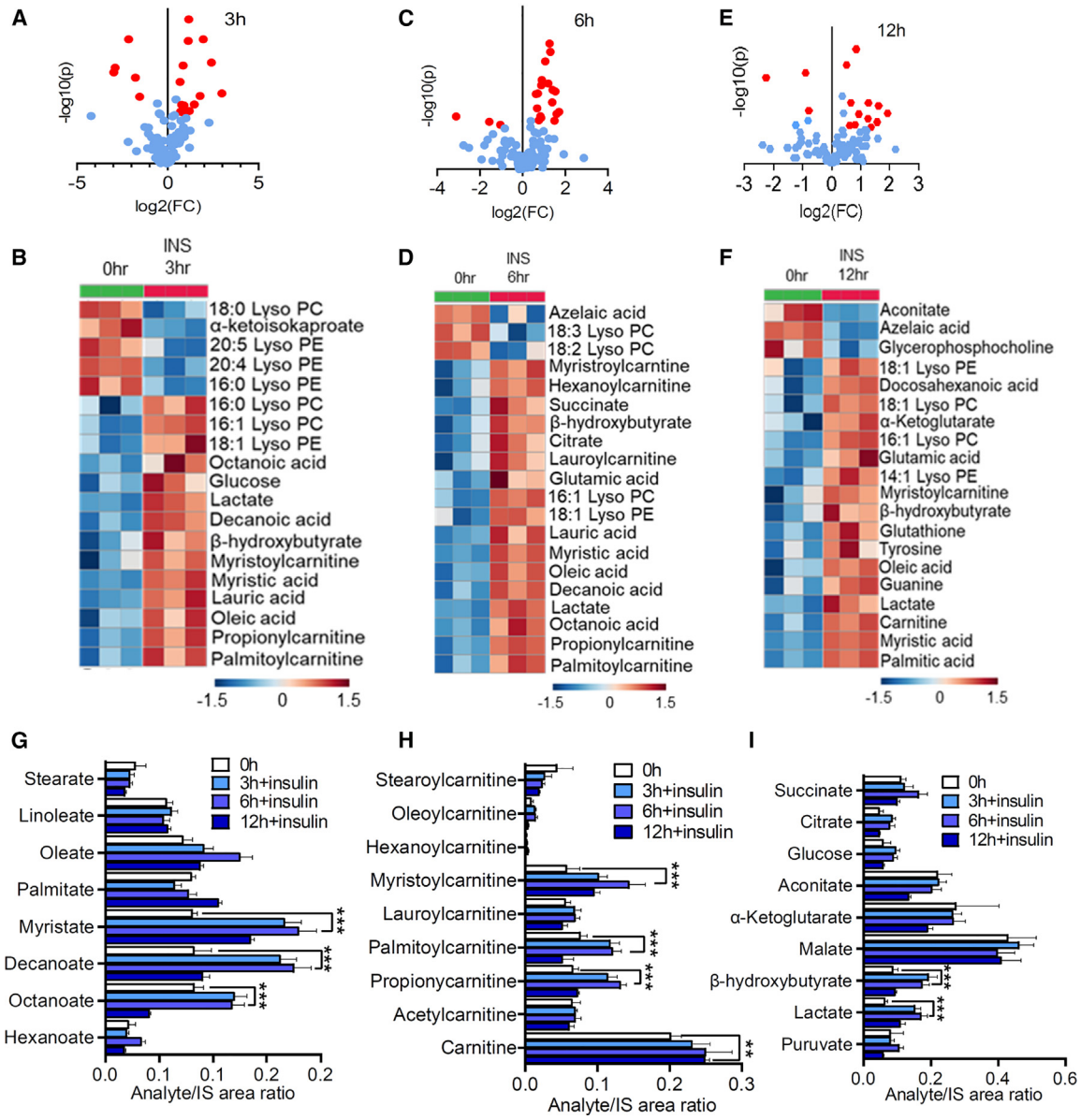

Figure 4. Insulin promotes the mobilization and metabolism of fatty acids in astrocytes

(A–I) Astrocytes were exposed to insulin for the indicated time points and metabolomics conducted on cell lysates. Volcano plots depicting metabolite fold changes in astrocyte cultures treated with insulin (200 nM) for (A) 3, (C) 6 and (E) 12h compared to vehicle. Red signifies metabolites that were modified in abundance following insulin treatment by 1.5 SD or greater and $p < 0.05$ or better. Heatmap projections showing the identity of metabolites with a group fold change >1.5 and $p < 0.05$ or better in astrocyte cultures treated with insulin for (B) 3, (D) 6, and (F) 12h compared to vehicle. Heat maps show the results from individual experiments. Targeted metabolomic analyses of (G) fatty acids, (H) fatty acylcarnitines and (I) TCA cycle products in astrocytes at the indicated time points following insulin exposure. Data are mean ± SEM from $n = 3$ independent experiments per condition. * = $p < 0.05$, ** = $p < 0.01$, *** = $p < 0.001$ ANOVA with Tukey post hoc comparisons.

(GFAP-IR KO). Baseline levels of glucose, pyruvate, and lactate were reduced, while myristate and palmitate were elevated in GFAP-IR KO mice compared to WT mice (Figures 5A and 5B). These data are consistent with an increased dependence on fatty acids as a fuel source in GFAP-IR KO mice.[49] In WT mice INI administration elevated hippocampal levels of glucose, lactate, citrate, β-hydroxybutyrate (Figure 5A), the fatty acids myristate and palmitate (Figure 5B) and the fatty acylcarnitine derivatives lauroylcarnitine, myristoylcarnitine, palmitoylcarnitine (Figure 5C). Levels of these metabolites were not modified by INI in GFAP-IR KO mice (Figures 5A–5C).

Insulin promotes palmitic acid oxidation in astrocytes

We determined the impact of insulin on the β-oxidation of palmitic acid in astrocytes using a heavy isotope ($^{13}C_{16}$) that yields 8 molecules of [2-^{13}C] acetyl-CoA that are substrates for the TCA

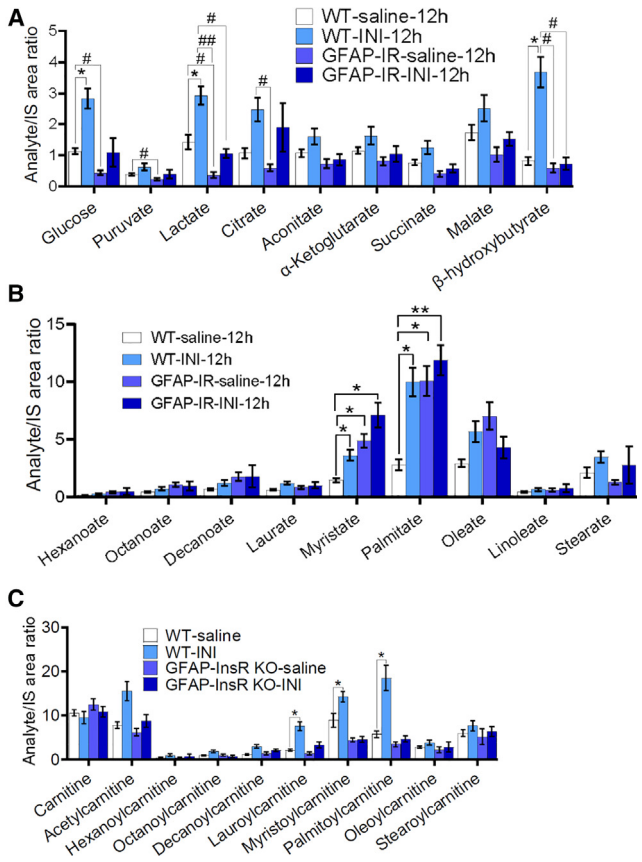

Figure 5. Astrocyte expressed insulin receptors are required for insulin to promote glucose uptake, glycolysis and fatty acid β-oxidation in brain

Wt and GFAP-InsR KO mice were administered saline or intranasal insulin (INI; 2.4 IU/nare, 4.8 IU total) and 12h later targeted metabolomics were conducted on hippocampal tissues to determine the impact of insulin on glucose and fatty acid metabolism.

(A) In Wt mice insulin increased glucose, lactate, citrate and β-hydroxybutyrate. In GFAP-InsR KO mice baseline levels of glucose and lactate were reduced while myristate and palmitate were increased compared with Wt. Insulin did not alter levels of these energetic substrates in GFAP-InsR KO mice. (B) In Wt mice insulin increased levels of myristate and palmitate. In GFAP-insR KO mice baseline levels of myristate and palmitate were elevated compared to Wt, but insulin did not modify levels of any fatty acid measured (C) In Wt mice insulin increased lauroylcarnitine, myristoylcarnitine, and palmitoylcarnitine. In GFAP-IR KO mice insulin did not modify levels of any acylcarnitine measured. Data are mean ± SEM from $n = 5$ independent experiments per condition. * = $p < 0.05$, ** = $p < 0.01$ compared to Wt saline. # = $p < 0.05$, ## = $p < 0.01$ for the indicated comparisons. ANOVA with Tukey post hoc comparisons.

cycle. The resulting TCA cycle metabolites are double labeled and detected as M+2 (two ^{13}C -enrichment) ions. The basal uptake of $^{13}C_{16}$ palmitate by astrocytes (Figure 6A) was increased ~10-fold by insulin (Figure 6B). In insulin exposed astrocytes $^{13}C_{16}$ palmitate was converted to ^{13}C-labelled palmitoyl-carnitine and the TCA cycle intermediates citrate, aconitate, α-ketoglutarate, succinate, and malate, demonstrating the use of palmitate by astrocytes as energy substrate through β-oxidation (Figure 6B). Inhibition of CPT1 by etomoxir prevented the oxidation of $^{13}C_{16}$ palmitate (Figure 6C). A schematic representation of $^{13}C_{16}$- palmitate oxidation resulting in acetyl-CoA that feeds into the TCA cycle is shown in Figure 6D. Using the Seahorse assay to measure mitochondrial functions we found that astrocytes pre-treated with insulin for 30min increased their total oxygen consumption rate (OCR; Figure 6E) and ATP levels (Figure 6F). Insulin increased lactate within 6h that was released into media and thus available for uptake and use by neurons as an energy substrate (Figure 6G). In neurons, insulin did not increase the uptake of $^{13}C_{16}$ and we did not detect the conversion of $^{13}C_{16}$ palmitate to palmitoyl-carnitine or any TCA cycle intermediates (Figures 6H and 6I). Likewise, insulin did not modify mitochondrial respiratory capacity in neurons (Figure 6J).

To directly compare the influence of insulin on glycolysis and fatty acid oxidation we exposed astrocytes simultaneously to $^{13}C_1$ glucose and $^{13}C_{16}$ palmitate with or without insulin for 3h. This allowed for the direct measurement of ^{13}C atom enrichment in TCA cycle products derived from either glucose or fatty acid oxidation. Insulin enhanced the uptake of both glucose and fatty acid in astrocytes. However, we observed a 2-mass-unit enrichment in TCA cycle products in astrocytes exposed to insulin, as demonstrating that the incorporation of 2-^{13}C acetyl CoA atoms resulted from the oxidation of fatty acids. Additionally, we observed a one-mass-unit enrichment in $^{13}C1$-lactate, suggesting that the $^{13}C_1$pyruvate derived from glucose oxidation is preferentially diverted to lactate production rather than entering the TCA cycle (Figure 7A). A schematic presentation of the ^{13}C isotopic flux analysis is shown in Figure 7B.

Insulin enhances long-term potentiation in the Schaffer collateral by mechanisms that require CPT1a and astrocyte insulin receptor expression

We next determined if there was a physiological consequence of insulin promoting the β-oxidation of fatty acids in astrocytes by measuring the effects of INI on LTP at the Schaffer collateral-commissural pathway (Figure 8A). Mice were treated with vehicle, INI, or pre-treated with a CPT1 inhibitor (etomoxir) 1h before INI or IN-Saline. Acute brain slices were prepared for LTP 6h after treatments. One minute after high frequency stimulation the magnitude of field excitatory postsynaptic potentials was increased in mice administered INI compared to IN-Saline. This LTP was sustained for at least 60min (Figure 8B). Inhibition of carnitine palmotoyltransferase 1 (CPT1) blocked the ability of INI to enhance LTP (Figures 8A and 8B). The CPT1 inhibitor alone had no effect on LTP. We then determined if astrocyte-expressed insulin receptors (IRs) were required for the enhancement of LTP by molecular knock down using a stereotactic delivered GFAP-shRNA$_{InsR}$. IR knock-down was confirmed by immunofluorescence (Figure 8C). INI did not enhance LTP in GFAP-shRNA$_{InsR}$ mice, compared with mice administered a scrambled shRNA (GFAP-shRNA$_{Scr}$) (Figures 8D and 8E). Field potential responses from CA1 at 60s following theta burst stimulation were analyzed by continuous wavelet transformation to deconstruct the temporal and frequency attributes of the compound waveform produced by the induction of LTP. The signal recorded from GFAP-shRNA$_{Scr}$ mice following INI exhibited an enhancement of the compressed frequency at roughly 1500 Hz in GFAP-shRNA$_{Scr}$ mice compared with GFAP-shRNA$_{InsR}$ mice (Figures 8F and 8G), suggesting a greater number of active

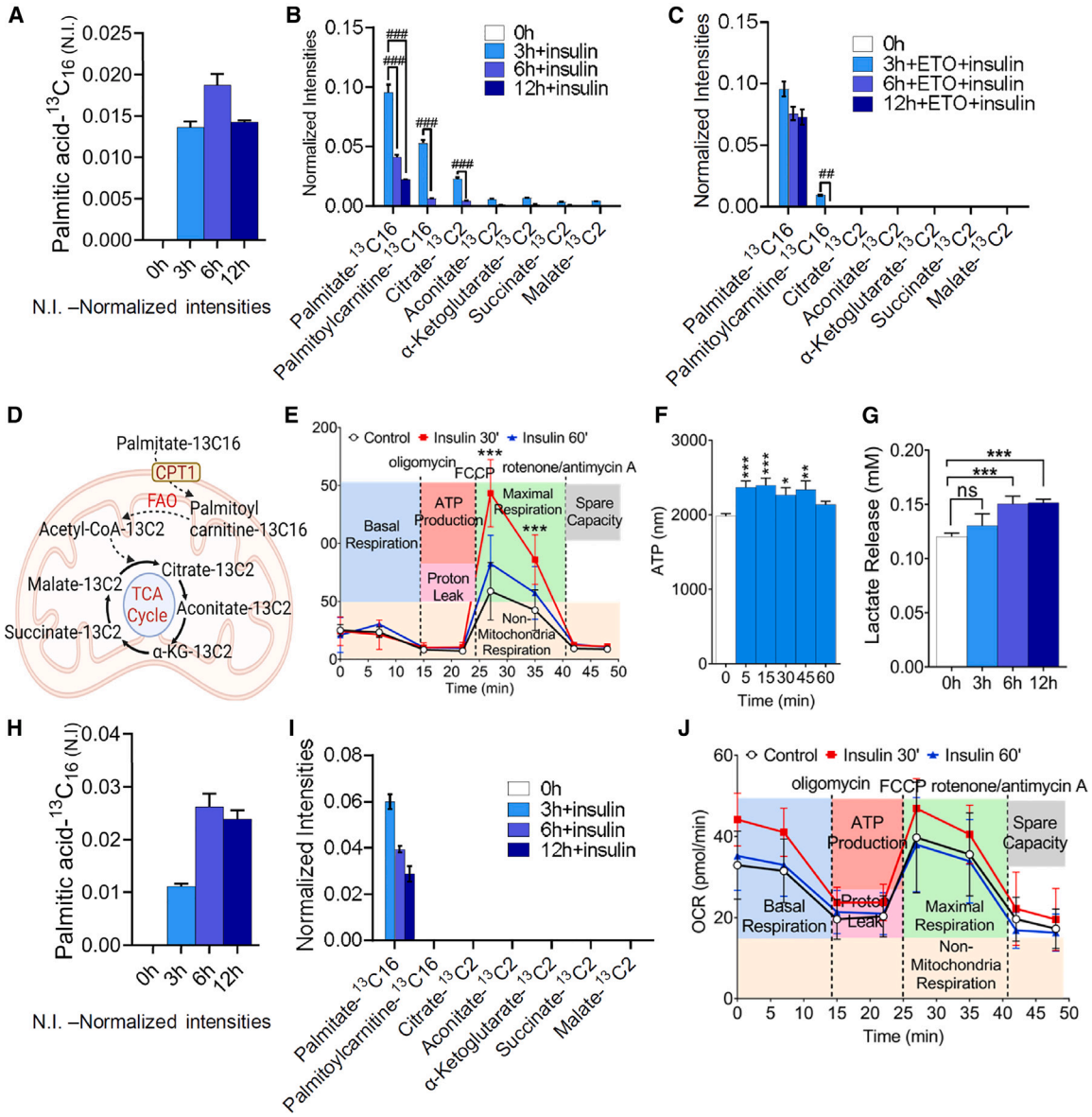

Figure 6. Insulin promotes the β-oxidation of fatty acids that are incorporated into the TCA cycle in astrocytes but not in neurons

Astrocytes were exposed to ^{13}C palmitate and the products of its metabolism were measured by mass spectrometry.

(A) Baseline uptake of ^{13}C-palmate in astrocytes over time.

(B) Insulin (200 nM) increased the uptake of ^{13}C-palmate and promoted oxidation in astrocytes, ^{13}C-was detected in palmitoyl-L-carnitine, citrate, aconitate, α-ketoglutarate, succinate and malate within 3h following insulin treatment with subsequent declines at the 6 and 12h timepoints.

(C) CPT1a inhibitor, etomoxir (10 μM) inhibited fatty acid oxidation, ^{13}C only detected in palmitate and palmitoylcarnitine within 3h of insulin exposure, that subsequently declined at 6 and 12h.

(D) Schematic showing the metabolism of ^{13}C-palmate.

(E) Mitochondrial respiration was measured by Seahorse in intact astrocytes following insulin treatment. Insulin increased the maximal respiratory capacity in astrocytes within 30 min of insulin exposure that declined to levels not different from control within 60 min

(F) Levels of ATP increased in astrocytes within 5 min of insulin exposure that were sustained for 45 min

(G) Insulin increased the release of lactate from astrocytes within 6h of treatment that was sustained for at-least 12h.

(H) In neurons the baseline uptake of ^{13}C-palmate increased from 3 to 6h and was sustained for up to 12h.

(I) Insulin doubled the uptake of ^{13}C-palmate in neurons that declined at 6 and 12h. ^{13}C-palmate was not metabolized to form any of the indicated downstream products in neurons.

(J) Insulin did not increase any aspect of mitochondrial respiratory function in neurons. Data are mean ± SEM from $n = 5$ independent experiments per condition. * = $p < 0.05$, ** = $p < 0.01$, *** = $p < 0.001$ compared with time 0, ## = $p < 0.01$, ### = $p < 0.001$ for the indicated comparisons. ANOVA with Tukey post hoc comparisons.

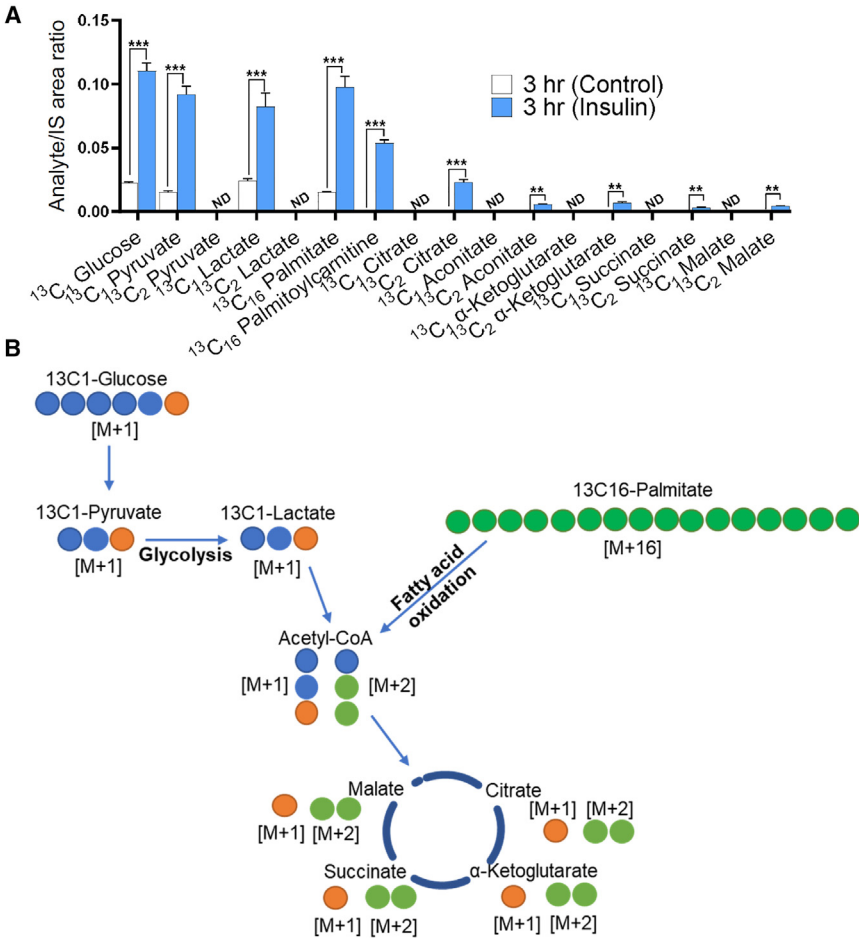

Figure 7. Insulin enhances the production of lactate from astrocytes by simultaneously increasing glycolysis to produce lactate, and by redirecting pyruvate created from the β-oxidation of fatty acids away from the TCA cycle to produce lactate

Astrocytes were exposed to $^{13}C_1$ glucose, and $^{13}C_{16}$ palmitate simultaneously with or without insulin, for 3h. The uptake of $^{13}C_1$ glucose, and $^{13}C_{16}$ palmitate and the intermediates in glycolysis, fatty acid oxidation and TCA cycle were measured by mass spectrometry.

(A) The levels of $^{13}C_1$ glucose, $^{13}C_1$ pyruvate, and, $^{13}C_1$ lactate were increased upon insulin exposure demonstrating the increased glycolysis pathway. while, the increased levels of $^{13}C_{16}$ palmitate, $^{13}C_{16}$ palmitoylcarnitine, and $^{13}C_2$ enrichment in TCA cycle intermediates demonstrating increased fatty acid oxidation, and incorporation of resultant acetyl-coA into TCA cycle. (B) Schmatic showing the metabolic pathway. Data are mean ± SEM from $n = 3$ independent experiments per condition. The symbols denote as follows: * = $p < 0.05$, ** = $p < 0.01$, *** = $p < 0.001$.

synaptic inputs contributed to enhanced LTP in mice administered INI. This compressed frequency was not apparent in GFAP-shRNA$_{InsR}$ mice administered INI, demonstrating that the insulin receptor on astrocytes was required to increase the number of active synaptic inputs (Figures 8F and 8G). These findings demonstrate that INI enhanced LTP through a mechanism that required astrocyte expressed insulin receptors.

DISCUSSION

Regardless of diabetic status, insulin levels in the cerebrospinal fluid (CSF) of patients with AD have produced mixed results. While some studies have reported decreased levels of insulin in the CSF (indicative of peripheral and central insulin resistance),[50] as well as, the expression of insulin receptors compared to non-AD control subjects,[51] others have found increased levels or no significant difference when compared to controls.[50,51] These discrepancies in findings could reflect different stages of disease progression, variations in patient populations, or methodological differences in the studies.

Insulin resistance has also been associated with an increased risk of developing Parkinson's disease[52,53] and has been associated with cognitive impairments in people infected with HIV.[54–58] Despite these known associations of insulin sensitivity with cognition, we know relatively little about the molecular regulation of brain bioenergetics by insulin.

Although we understand a great deal about how insulin regulates energy metabolism in peripheral tissues, we know very little about the roles of insulin in regulating brain bioenergetics. Here we provide evidence that insulin promotes a shift of energy substrate preference in astrocytes to favor the β-oxidation of fatty acids. This shift in energy substrate preference was not apparent in neurons treated with insulin. While we do not fully understand the biological consequences of this phenomenon, we demonstrated that insulin enhanced LTP by mechanisms dependent on astrocyte-expressed insulin receptors on astrocytes and CPT1a.

INI produced time-dependent changes in the expression of genes regulating multiple signaling pathways in the mouse brain. Genes rapidly upregulated following INI were associated with neurotrophic effects,[59,60] consistent with known functions of insulin to protect neurons and stabilize synapses.[16,61] Within 1h of INI treatment, the expression of genes regulating metabolic pathways and functions associated with glucose metabolism were increased. These data expand on previous findings that demonstrated local insulin injection into the brain increased hippocampal extracellular glucose and lactate concentrations.[62] Within 1h of INI the expression of genes involved with lipid storage and secretion of fatty acids were increased, suggesting that insulin promotes the mobilization of fatty acids in the brain. Six hours following INI there was a robust and preferential upregulation of pathways involved in lipid and fatty acid metabolism. Together these data demonstrate insulin promotes a metabolic switch from glucose to fatty acid utilization in astrocytes, but not in neurons. We believe this insulin-induced switch in

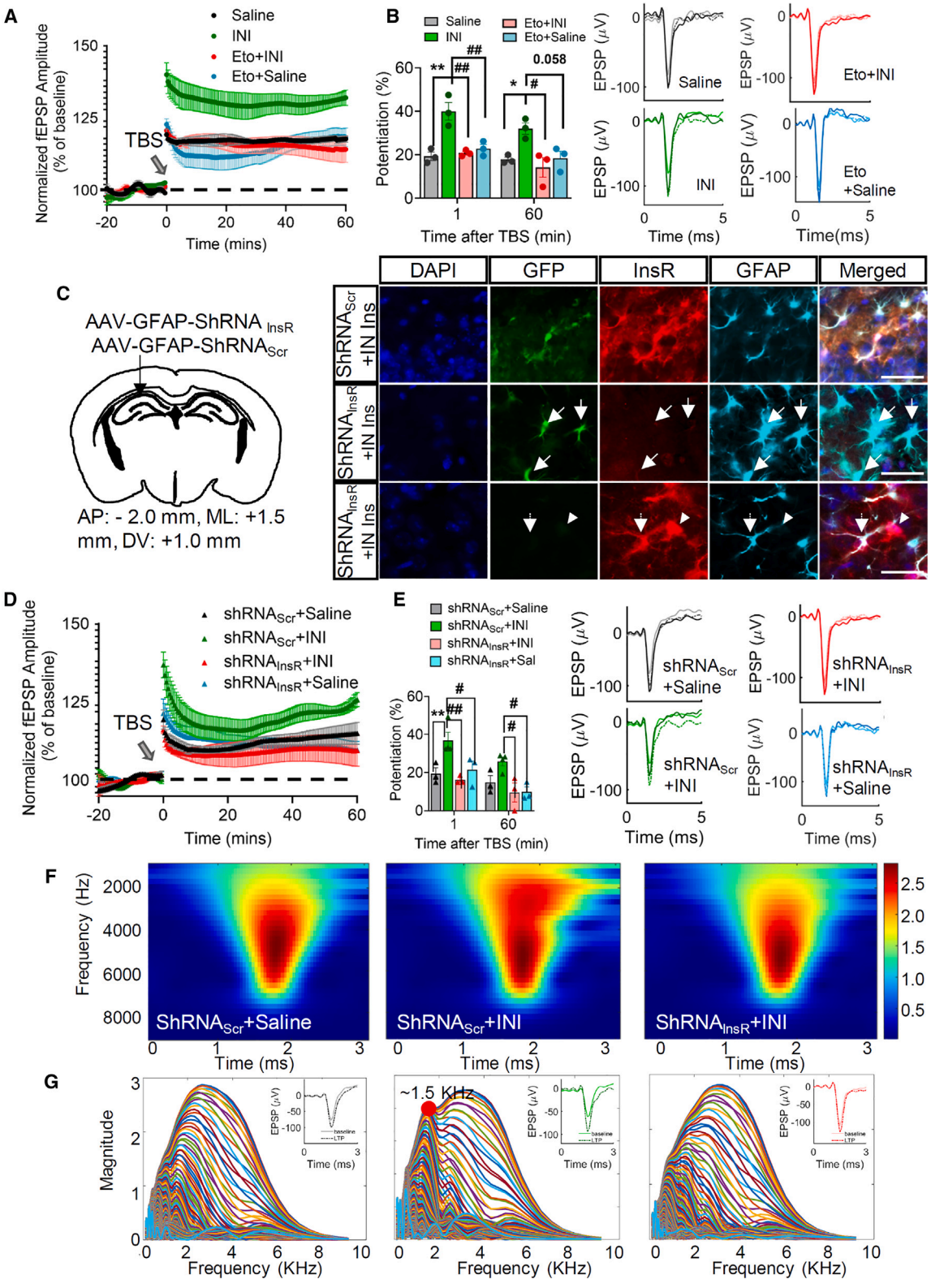

(legend on next page)

astrocyte energy substrate preference occurs to provide neurons with the energy substrates required to upregulate trophic and protective functions that are directly and rapidly activated by insulin. Our data suggest that insulin selectively promotes fatty acid oxidation in astrocytes to generate pyruvate that in the presence of insulin is preferentially diverted to lactate production rather than entering the TCA cycle.

Our results from primary hippocampal neuronal cultures confirmed the ability of INI to promote protective and trophic responses. Direct insulin treatment of neurons increased the expression of genes involved in synaptogenesis, serotonin degradation, glutathione mediated detoxification, sirtuin signaling, IL-15 production, and CREB signaling. The effects of insulin on synaptogenesis are well known and documented. Increased nicotine, nicotinamide metabolism, and phospholipid biosynthesis we observed in neurons exposed to insulin suggest that insulin promoted metabolism essential for membrane biogenesis. The upregulation of glutathione detoxification in neurons is consistent with an increased need to detoxify hydroperoxides that are generated by oxidative reactions. Sirtuins are a family of NAD-dependent histone deacetylases that are activated under conditions of calorie restriction.[63] Sirtuin 1 (SIRT1) is the most studied NAD-dependent histone deacetylases that have been shown to play a role in glucose and lipid metabolism. SIRT1 induces a glucose-dependent insulin secretion from pancreatic beta cells and directly stimulates insulin signaling pathways in insulin-sensitive organs including the brain.[64] In the brain, Sirt1 negatively regulates hypothalamic insulin signaling which can result in systemic insulin resistance.[65] IL-15 is an inflammatory cytokine that slows the uptake of GABA with consequent improvements in memory function.[66] CREB signaling is well known to promote the expression of genes associated with several neuronal survival pathways.[67] At later time points following insulin exposure genes associated with axonal guidance, actin cytoskeleton signaling and Rho family GTPases were also increased consistent with synaptic development and stabilization. This insulin-induced shift in neuronal gene expression is consistent with our data demonstrating that insulin enhanced LTP by increasing the number of active synaptic inputs. Since LTP has been shown to require astrocyte to neuron lactate transport,[68,69] it is likely that the insulin-induced release of lactate from astrocytes fueled the enhancement of LTP. This observation challenges the current notion that astrocytes only release lactate under conditions of glycogenolysis. However, further experimentation is required to establish the mechanisms by which insulin promotes the diversion of lactate from the TCA cycle in astrocytes.

Compared with cortical neurons, astrocytes are enriched with genes coding for enzymes involved in fatty acid oxidation.[70] Here we found that insulin selectively increased the expression of genes in astrocytes associated with fatty acid metabolism, with concurrent increases in several fatty acids, their fatty acyl-carnitine derivatives and maximal mitochondrial respiratory capacity. In metabolic flux experiments, we demonstrated that insulin promoted the conversion of $_{13}C^{16}$ palmitate to ^{13}C-labelled palmitoyl-carnitine and the TCA cycle intermediates citrate, aconitate, α-ketoglutarate, succinate, and malate in astrocytes, but not in neurons. This directly demonstrates the use of palmitate by astrocytes as an energy substrate through β-oxidation. This insulin-induced upregulation of β-oxidation in astrocytes was sustained for at least 6h, as evidenced by the increased expression of several proteins involved in fatty acid transport and handling including phospholipases that hydrolyze phospholipids on sn-2 position to generate free unsaturated fatty acids, and triacylglycerols that are hydrolyzed by lipases to generate free fatty acids. Although the generation of free fatty acids from triacylglycerols for use as an energy substrate is known to occur in adipocytes and other peripheral organs, this is the first demonstration of this pathway in astrocytes.

In a tandem metabolic flux experiment, we used $^{13}C_1$ glucose and $^{13}C_{16}$ palmitate to directly determine if ^{13}C containing TCA cycle metabolites were generated from either glucose or fatty acid oxidation. Our data demonstrate that exposing astrocytes to insulin promoted the production of TCA cycle metabolites that were derived from the oxidation of fatty acids. We also observed that $^{13}C_1$pyruvate derived from glucose oxidation was diverted to lactate production rather than entering the

Figure 8. Carnitine palmitoyltransferase-1 and the insulin receptor on astrocytes are critical for the effects of insulin to promote long-term potentiation in neurons

(A) Summary tracings showing field excitatory postsynaptic potentials following high frequency stimulation of the Schaffer collateral in brain slices from mice administered intranasal saline (Saline; black traces), intranasal insulin (green traces) (INI; 2.4 IU/nare, 4.8 IU total; green traces) or intranasal delivery of the CPT-1 inhibitor Etomoxir (0.16μg/nair; 0.322μg/total) and insulin (Eto-INI; red traces) and saline (Eto-Sal; blue traces).

(B) Summary data showing percent of potentiation and representative traces for the indicated treatments.

(C) An adenoviral vector containing a GFAP driven GFP-labelled shRNA directed to reduced expression of the type 1 insulin receptor ($shRNA_{InsR}$) or a scrambled GFP-labelled shRNA ($shRNA_{Scr}$) was administered to the indicated coordinates 48h prior to experimentation. Immunostaining shows nuclear staining (Dapi; blue), green fluorescent protein (GFP; green), the insulin receptor type 1 (InsR; red) and the merged images where co-localized GFP, InsR and GFAP appear as white. Solid Arrows: Indicate astrocytes transduced with AAV-$shRNA_{Ins.}$ Dashed Arrows: Indicate astrocytes not transduced with AAV-$shRNA_{InsR}$. Arrowheads: Indicate non-astrocytic cells expressing InsR.

(D) Summary tracings showing field excitatory postsynaptic potentials following high frequency stimulation of the Schaffer collateral in brain slices from mice administered shRNAScr + saline ($shRNA_{Scr}$+saline; black traces), shRNAScr + intranasal insulin ($shRNA_{InsR}$+INI; green traces),$shRNA_{InsR}$ + intranasal insulin ($shRNA_{InsR}$+INI; red traces) or $shRNA_{InsR}$ + Saline ($shRNA_{InsR}$ +IN-Sal; blue traces).

(E) Summary data showing percent of potentiation and representative traces for the indicated conditions.

(F) Spectral maps and (G) frequency traces depicting the temporal and frequency attributes of the compound waveforms associated with field potentials showing an enhancement of the compressed frequency in $shRNA_{Scr}$ administered insulin at roughly 1500 Hz compared with $shRNA_{Scr}$ mice administered intranasal saline suggesting additional information being rendered following induction of LTP for mice with administration of Insulin. Data are mean ± SEM from $n = 3$ independent experiments per condition. * = $p < 0.05$, ** = $p < 0.01$ increased compared to saline. # = $p < 0.05$, ## = $p < 0.01$ compared to INI. ANOVA with Tukey post hoc comparisons. Scale bar, 20 μm.

TCA cycle. Although we do not fully understand the mechanism by which insulin promotes this unconventional metabolic flux in astrocytes, we determined that the production of lactate from pyruvate was required for insulin-induced LTP.

Differences in how neurons and astrocytes respond to insulin may foster their metabolic cooperation.[71] For example, fatty acid oxidation in astrocytes has been shown to co-occur with glycolysis and is inhibited by glutamate.[70,72] These data suggest that neuronal activity may regulate the energy substrate preference of astrocytes. High neuronal activity may promote a metabolic switch in astrocytes to favor the β-oxidation of fatty acids in order to provide an additional and sustained supply of lactate that is readily used by neurons for fuel. We can envision three possible mechanisms by which insulin signaling in astrocytes promotes the production of lactate. Insulin treatment promotes glucose uptake in astrocytes in addition to the increased utilization of fatty acids. Glucose may not be completely utilized for energy production and may instead be stored as glycogen within astrocytes. Stored glycogen provides the substrate for a sustained breakdown of glucose that undergoes glycolysis to produce lactate. Indeed, it has been demonstrated that glucose can be used by astrocytes for glycolysis or the glycogen shunt pathway.[73] It is also possible that a series of time-dependent mechanisms contribute to insulin-induced increases of lactate production in astrocytes. For example, the initial production of lactate may be due to glucose uptake and glycolysis (pyruvate fermentation to lactate in the cytosol), while at later time points when available glucose has been depleted, lactate is derived from the breakdown of glycogen, and/or metabolic re-programming in response to the reduced utilization of pyruvate derived acetyl CoA resulting in a consequent increase of glycolysis to produce lactate. Further studies are needed to elucidate precisely how the induction of the β-oxidation of fatty acids in astrocytes is connected to gluconeogenesis, and how the production of lactate is regulated in astrocytes in response to insulin.

In summary, we demonstrate that insulin promotes a metabolic reprograming in astrocytes that shifts the energy substrate preference to fatty acids. This insulin evoked metabolic switch in astrocytes involves a time-dependent and sequential shift in the expression of genes involved in the mobilization and utilization of fatty acids. We found that insulin promotes the uptake of glucose and fatty acids in astrocytes while shifting their metabolic preference from glucose to fatty acids. This occurs through a sequential shift in the expression of genes associated with fatty acid uptake, synthesis, transport, and metabolism. Under these conditions the fatty acids in astrocytes are converted into TCA cycle intermediates in sufficient quantity to satisfy astrocyte energy demands. This allows pyruvate, derived from glucose, to be shuttled toward the production of lactate that is a preferred fuel for neurons. This shift in astrocyte energy substrate preference is required for insulin to enhance long-term potentiation in the Schaffer collateral. These findings establish a homeostatic mechanism where insulin promotes LTP by switching the energy substrate preference of astrocytes to fatty acids so that glucose is shuttled to the production of lactate.

One consequence of this insulin-induced metabolic shift in astrocytes is the sustained production and release of lactate from unconventional sources to promote LTP. Since reductions in brain insulin sensitivity are common to several neurodegenerative conditions, these findings suggest that impairments of learning and memory may involve reductions in the ability of astrocytes to β-oxidize fatty acids that ultimately are converted to lactate.

Limitations of the study

This study contributes to the growing literature that demonstrates astrocytes are capable of metabolizing fatty acids. These findings do not change the long-standing notion that glucose is the primary energy substrate in the brain, but instead increase our understanding of substrates available for energy production in the brain. There are several opportunities identified by the current study. Our *in vivo* studies were conducted using a single brain region. While this is informative of overall metabolism for that brain region, from this approach we cannot determine the contributions of individual cell types to the observed shifts in metabolic profiles that occur in response to insulin. It is also likely that there are regional differences in the types of substrates that can be used by astrocytes for oxidation, in addition to regional differences in insulin sensitivity. Future studies will need to address these questions to fully appreciate the mechanisms of energy substrate switching in the brain.

RESOURCE AVAILABILITY

Lead contact

Requests for information, resources, or reagents should be directed to Dr. Norman Haughey (nhaughey@tulane.edu).

Materials availability

This study did not generate any unique reagents.

Data and code availability

The RNAseq data generated in this study is publicly available at Gene Express Omnibus (GSE280416 and GSE280417). MATLAB code used to analyze the LTP data is available on the laboratory website (https://haugheylab.org/) under the software tab.

ACKNOWLEDGMENTS

This work was supported by the National Institutes of Health grants: P01MH105280, AG057420, DA04039, DA052272, MH110246 to NJH, and a Bloomberg Distinguished Professorship to RSA. We thank Dr. Meina Wang for her valuable contributions to support this study.

AUTHOR CONTRIBUTIONS

Conceptualization and methodology: N.J.H.; experiments, P.D., S.S.K., S.G., and S.Y.W.; data analysis, P.D., S.S.K., S.G., and S.W.Y.; writing – initial draft, N.J.H., B.T., R.S.A., and P.D.; writing – review and editing, N.J.H., B.T., R.S.A., P.D., S.S.K., S.G., Z.L., A.H., and S.Y.W.

DECLARATION OF INTERESTS

The authors declare no competing interests.

STAR★METHODS

Detailed methods are provided in the online version of this paper and include the following:

- KEY RESOURCES TABLE
- EXPERIMENTAL MODEL AND STUDY PARTICIPANT DETAILS

SUPPLEMENTAL INFORMATION

Supplemental information can be found online at https://doi.org/10.1016/j.isci.2024.111642.

Received: June 20, 2024
Revised: August 21, 2024
Accepted: December 17, 2024
Published: January 20, 2025

REFERENCES

1. Chen, L., Chen, X.W., Huang, X., Song, B.L., Wang, Y., and Wang, Y. (2019). Regulation of glucose and lipid metabolism in health and disease. Sci. China Life Sci. *62*, 1420–1458. https://doi.org/10.1007/s11427-019-1563-3.
2. McGarry, J.D. (1998). Glucose-fatty acid interactions in health and disease. Am. J. Clin. Nutr. *67*, 500S–504S. https://doi.org/10.1093/ajcn/67.3.500S.
3. Adibhatla, R.M., and Hatcher, J.F. (2008). Altered lipid metabolism in brain injury and disorders. Subcell. Biochem. *49*, 241–268. https://doi.org/10.1007/978-1-4020-8831-5_9.
4. Mergenthaler, P., Lindauer, U., Dienel, G.A., and Meisel, A. (2013). Sugar for the brain: the role of glucose in physiological and pathological brain function. Trends Neurosci. *36*, 587–597. https://doi.org/10.1016/j.tins.2013.07.001.
5. Ioannou, M.S., Jackson, J., Sheu, S.H., Chang, C.L., Weigel, A.V., Liu, H., Pasolli, H.A., Xu, C.S., Pang, S., Matthies, D., et al. (2019). Neuron-Astrocyte Metabolic Coupling Protects against Activity-Induced Fatty Acid Toxicity. Cell *177*, 1522–1535.e14. https://doi.org/10.1016/j.cell.2019.04.001.
6. Qi, G., Mi, Y., Shi, X., Gu, H., Brinton, R.D., and Yin, F. (2021). ApoE4 Impairs Neuron-Astrocyte Coupling of Fatty Acid Metabolism. Cell Rep. *34*, 108572. https://doi.org/10.1016/j.celrep.2020.108572.
7. Van Houten, B. (2019). Huntington's Disease: Astrocytes Shift to Fatty Acid Metabolism. Trends Endocrinol. Metab. *30*, 575–577. https://doi.org/10.1016/j.tem.2019.07.019.
8. Polyzos, A.A., Lee, D.Y., Datta, R., Hauser, M., Budworth, H., Holt, A., Mihalik, S., Goldschmidt, P., Frankel, K., Trego, K., et al. (2019). Metabolic Reprogramming in Astrocytes Distinguishes Region-Specific Neuronal Susceptibility in Huntington Mice. Cell Metab. *29*, 1258–1273.e11. https://doi.org/10.1016/j.cmet.2019.03.004.
9. Gottschalk, S., and Zwingmann, C. (2009). Altered fatty acid metabolism and composition in cultured astrocytes under hyperammonemic conditions. J. Neurochem. *109* (*Suppl 1*), 258–264. https://doi.org/10.1111/j.1471-4159.2009.05985.x.
10. Natarajaseenivasan, K., Cotto, B., Shanmughapriya, S., Lombardi, A.A., Datta, P.K., Madesh, M., Elrod, J.W., Khalili, K., and Langford, D. (2018). Astrocytic metabolic switch is a novel etiology for Cocaine and HIV-1 Tat-mediated neurotoxicity. Cell Death Dis. *9*, 415. https://doi.org/10.1038/s41419-018-0422-3.
11. Schonfeld, P., and Reiser, G. (2013). Why does brain metabolism not favor burning of fatty acids to provide energy? Reflections on disadvantages of the use of free fatty acids as fuel for brain. J. Cereb. Blood Flow. Metab. *33*, 1493–1499. https://doi.org/10.1038/jcbfm.2013.128.
12. Panov, A., Orynbayeva, Z., Vavilin, V., and Lyakhovich, V. (2014). Fatty acids in energy metabolism of the central nervous system. BioMed Res. Int. *2014*, 472459. https://doi.org/10.1155/2014/472459.
13. Hardie, D.G. (2012). Organismal carbohydrate and lipid homeostasis. Cold Spring Harb. Perspect. Biol. *4*, a006031. https://doi.org/10.1101/cshperspect.a006031.
14. Ghasemi, R., Haeri, A., Dargahi, L., Mohamed, Z., and Ahmadiani, A. (2013). Insulin in the brain: sources, localization and functions. Mol. Neurobiol. *47*, 145–171. https://doi.org/10.1007/s12035-012-8339-9.
15. Unger, J.W., Livingston, J.N., and Moss, A.M. (1991). Insulin receptors in the central nervous system: localization, signalling mechanisms and functional aspects. Prog. Neurobiol. *36*, 343–362. https://doi.org/10.1016/0301-0082(91)90015-s.
16. Pomytkin, I., Costa-Nunes, J.P., Kasatkin, V., Veniaminova, E., Demchenko, A., Lyundup, A., Lesch, K.P., Ponomarev, E.D., and Strekalova, T. (2018). Insulin receptor in the brain: Mechanisms of activation and the role in the CNS pathology and treatment. CNS Neurosci. Ther. *24*, 763–774. https://doi.org/10.1111/cns.12866.
17. Woods, S.C., Seeley, R.J., Baskin, D.G., and Schwartz, M.W. (2003). Insulin and the blood-brain barrier. Curr. Pharm. Des. *9*, 795–800. https://doi.org/10.2174/1381612033455323.
18. Morton, G.J., Cummings, D.E., Baskin, D.G., Barsh, G.S., and Schwartz, M.W. (2006). Central nervous system control of food intake and body weight. Nature *443*, 289–295. https://doi.org/10.1038/nature05026.
19. Ketterer, C., Tschritter, O., Preissl, H., Heni, M., Häring, H.U., and Fritsche, A. (2011). Insulin sensitivity of the human brain. Diabetes Res. Clin. Pract. *93* (*Suppl 1*), S47–S51. https://doi.org/10.1016/S0168-8227(11)70013-4.
20. Akhtar, A., and Sah, S.P. (2020). Insulin signaling pathway and related molecules: Role in neurodegeneration and Alzheimer's disease. Neurochem. Int. *135*, 104707. https://doi.org/10.1016/j.neuint.2020.104707.
21. Gonzalez-Reyes, R.E., Aliev, G., Avila-Rodrigues, M., and Barreto, G.E. (2016). Alterations in Glucose Metabolism on Cognition: A Possible Link Between Diabetes and Dementia. Curr. Pharmaceut. Des. *22*, 812–818. https://doi.org/10.2174/1381612822666151209152013.
22. Thomas, K.R., Bangen, K.J., Weigand, A.J., Edmonds, E.C., Sundermann, E., Wong, C.G., Eppig, J., Werhane, M.L., Delano-Wood, L., and Bondi, M.W.; Alzheimer's Disease Neuroimaging Initiative (2020). Type 2 Diabetes Interacts With Alzheimer Disease Risk Factors to Predict Functional Decline. Alzheimer Dis. Assoc. Disord. *34*, 10–17. https://doi.org/10.1097/WAD.0000000000000332.
23. Zilliox, L.A., Chadrasekaran, K., Kwan, J.Y., and Russell, J.W. (2016). Diabetes and Cognitive Impairment. Curr. Diab. Rep. *16*, 87. https://doi.org/10.1007/s11892-016-0775-x.
24. Martínez, M., and Mougan, I. (1998). Fatty Acid Composition of Human Brain Phospholipids During Normal Development. J. Neurochem. *71*, 2528–2533. https://doi.org/10.1046/j.1471-4159.1998.71062528.x.
25. Barber, C.N., and Raben, D.M. (2019). Lipid Metabolism Crosstalk in the Brain: Glia and Neurons. Front. Cell. Neurosci. *13*, 212. https://doi.org/10.3389/fncel.2019.00212.
26. Chen, C.T., Haven, S., Lecaj, L., Borgstrom, M., Torabi, M., SanGiovanni, J.P., and Hibbeln, J.R. (2020). Brain PUFA Concentrations Are Differentially Affected by Interactions of Diet, Sex, Brain Regions, and Phospholipid Pools in Mice. J. Nutr. *150*, 3123–3132. https://doi.org/10.1093/jn/nxaa307.

27. Montecillo-Aguado, M., Tirado-Rodriguez, B., Tong, Z., Vega, O.M., Morales-Martínez, M., Abkenari, S., Pedraza-Chaverri, J., and Huerta-Yepez, S. (2020). Importance of the Role of ω-3 and ω-6 Polyunsaturated Fatty Acids in the Progression of Brain Cancer. Brain Sci. *10*, 381. https://doi.org/10.3390/brainsci10060381.

28. Lee, J., Choi, J., Scafidi, S., and Wolfgang, M.J. (2016). Hepatic Fatty Acid Oxidation Restrains Systemic Catabolism during Starvation. Cell Rep. *16*, 201–212. https://doi.org/10.1016/j.celrep.2016.05.062.

29. Grynberg, A., and Demaison, L. (1996). Fatty acid oxidation in the heart. J. Cardiovasc. Pharmacol. *28*, S11–S17. https://doi.org/10.1097/00005344-199600003-00003.

30. Fritzen, A.M., Lundsgaard, A.-M., and Kiens, B. (2020). Tuning fatty acid oxidation in skeletal muscle with dietary fat and exercise. Nat. Rev. Endocrinol. *16*, 683–696. https://doi.org/10.1038/s41574-020-0405-1.

31. Eraso-Pichot, A., Brasó-Vives, M., Golbano, A., Menacho, C., Claro, E., Galea, E., and Masgrau, R. (2018). GSEA of mouse and human mitochondriomes reveals fatty acid oxidation in astrocytes. Glia *66*, 1724–1735. https://doi.org/10.1002/glia.23330.

32. Schulz, J.G., Laranjeira, A., Van Huffel, L., Gärtner, A., Vilain, S., Bastianen, J., Van Veldhoven, P.P., and Dotti, C.G. (2015). Glial β-Oxidation regulates Drosophila Energy Metabolism. Sci. Rep. *5*, 7805. https://doi.org/10.1038/srep07805. https://www.nature.com/articles/srep07805#supplementary-information.

33. Suzuki, A., Stern, S.A., Bozdagi, O., Huntley, G.W., Walker, R.H., Magistretti, P.J., and Alberini, C.M. (2011). Astrocyte-Neuron Lactate Transport Is Required for Long-Term Memory Formation. Cell *144*, 810–823. https://doi.org/10.1016/j.cell.2011.02.018.

34. Deme, P., Rojas, C., Slusher, B.S., Rais, R., Afghah, Z., Geiger, J.D., and Haughey, N.J. (2020). Bioenergetic adaptations to HIV infection. Could modulation of energy substrate utilization improve brain health in people living with HIV-1? Exp. Neurol. *327*, 113181. https://doi.org/10.1016/j.expneurol.2020.113181.

35. Morris, A.A.M. (2005). Cerebral ketone body metabolism. J. Inherit. Metab. Dis. *28*, 109–121. https://doi.org/10.1007/s10545-005-5518-0.

36. Duran, J., Gruart, A., López-Ramos, J.C., Delgado-García, J.M., and Guinovart, J.J. (2019). Glycogen in Astrocytes and Neurons: Physiological and Pathological Aspects. Adv. Neurobiol. *23*, 311–329. https://doi.org/10.1007/978-3-030-27480-1_10.

37. Smolič, T., Tavčar, P., Horvat, A., Černe, U., Halužan Vasle, A., Tratnjek, L., Kreft, M.E., Scholz, N., Matis, M., Petan, T., et al. (2021). Astrocytes in stress accumulate lipid droplets. Glia *69*, 1540–1562. https://doi.org/10.1002/glia.23978.

38. Machler, P., Wyss, M.T., Elsayed, M., Stobart, J., Gutierrez, R., von Faber-Castell, A., Kaelin, V., Zuend, M., San Martin, A., Romero-Gomez, I., et al. (2016). In Vivo Evidence for a Lactate Gradient from Astrocytes to Neurons. Cell Metab *23*, 94–102. https://doi.org/10.1016/j.cmet.2015.10.010.

39. Shen, J., Petersen, K.F., Behar, K.L., Brown, P., Nixon, T.W., Mason, G.F., Petroff, O.A., Shulman, G.I., Shulman, R.G., and Rothman, D.L. (1999). Determination of the rate of the glutamate/glutamine cycle in the human brain by in vivo ^{13}C NMR. Proc. Natl. Acad. Sci. USA *96*, 8235–8240. https://doi.org/10.1073/pnas.96.14.8235.

40. Ioannou, M.S., Jackson, J., Sheu, S.-H., Chang, C.-L., Weigel, A.V., Liu, H., Pasolli, H.A., Xu, C.S., Pang, S., Hess, H.F., et al. (2018). Neuron-astrocyte metabolic coupling during neuronal stimulation protects against fatty acid toxicity. Preprint at bioRxiv. https://doi.org/10.1101/465237.

41. Hilse, K.E., Rupprecht, A., Egerbacher, M., Bardakji, S., Zimmermann, L., Wulczyn, A.E.M.S., and Pohl, E.E. (2018). The Expression of Uncoupling Protein 3 Coincides With the Fatty Acid Oxidation Type of Metabolism in Adult Murine Heart. Front. Physiol. *9*, 747.

42. Fernandez, A.M., Hernandez, E., Guerrero-Gomez, D., Miranda-Vizuete, A., and Torres Aleman, I. (2018). A network of insulin peptides regulate glucose uptake by astrocytes: Potential new druggable targets for brain hypometabolism. Neuropharmacology *136*, 216–222. https://doi.org/10.1016/j.neuropharm.2017.08.034.

43. Mueckler, M. (1994). Facilitative glucose transporters. Eur. J. Biochem. *219*, 713–725.

44. Heidenrich, K.A., Gilmore, P.R., and Garvey, W.T. (1989). Glucose transport in primary cultured neurons. J. Neurosci. Res. *22*, 397–407. https://doi.org/10.1002/jnr.490220405.

45. Proia, P., Di Liegro, C.M., Schiera, G., Fricano, A., and Di Liegro, I. (2016). Lactate as a Metabolite and a Regulator in the Central Nervous System. Int. J. Mol. Sci. *17*, 1450. https://doi.org/10.3390/ijms17091450.

46. Conlay, L.A., and Zeisel, S.H. (1982). Neurotransmitter precursors and brain function. Neurosurgery *10*, 524–529. https://doi.org/10.1227/00006123-198204000-00021.

47. Braidy, N., Berg, J., Clement, J., Khorshidi, F., Poljak, A., Jayasena, T., Grant, R., and Sachdev, P. (2019). Role of Nicotinamide Adenine Dinucleotide and Related Precursors as Therapeutic Targets for Age-Related Degenerative Diseases: Rationale, Biochemistry, Pharmacokinetics, and Outcomes. Antioxid. Redox Signal. *30*, 251–294. https://doi.org/10.1089/ars.2017.7269.

48. Lauwers, E., Goodchild, R., and Verstreken, P. (2016). Membrane Lipids in Presynaptic Function and Disease. Neuron *90*, 11–25. https://doi.org/10.1016/j.neuron.2016.02.033.

49. Garcia-Caceres, C., Quarta, C., Varela, L., Gao, Y., Gruber, T., Legutko, B., Jastroch, M., Johansson, P., Ninkovic, J., Yi, C.X., et al. (2016). Astrocytic Insulin Signaling Couples Brain Glucose Uptake with Nutrient Availability. Cell *166*, 867–880. https://doi.org/10.1016/j.cell.2016.07.028.

50. Stanley, M., Macauley, S.L., and Holtzman, D.M. (2016). Changes in insulin and insulin signaling in Alzheimer's disease: cause or consequence? J. Exp. Med. *213*, 1375–1385. https://doi.org/10.1084/jem.20160493.

51. Steen, E., Terry, B.M., Rivera, E.J., Cannon, J.L., Neely, T.R., Tavares, R., Xu, X.J., Wands, J.R., and de la Monte, S.M. (2005). Impaired insulin and insulin-like growth factor expression and signaling mechanisms in Alzheimer's disease–is this type 3 diabetes? J. Alzheimers Dis. *7*, 63–80. https://doi.org/10.3233/jad-2005-7107.

52. Dias, V., Junn, E., and Mouradian, M.M. (2013). The role of oxidative stress in Parkinson's disease. J. Parkinsons Dis. *3*, 461–491. https://doi.org/10.3233/JPD-130230.

53. Guo, J.D., Zhao, X., Li, Y., Li, G.R., and Liu, X.L. (2018). Damage to dopaminergic neurons by oxidative stress in Parkinson's disease (Review). Int. J. Mol. Med. *41*, 1817–1825. https://doi.org/10.3892/ijmm.2018.3406.

54. Pedro, M.N., Rocha, G.Z., Guadagnini, D., Santos, A., Magro, D.O., Assalin, H.B., Oliveira, A.G., Pedro, R.d.J., and Saad, M.J.A. (2018). Insulin Resistance in HIV-Patients: Causes and Consequences. Front. Endocrinol. *9*, 514. https://doi.org/10.3389/fendo.2018.00514.

55. Gutierrez, A.D., and Balasubramanyam, A. (2012). Dysregulation of glucose metabolism in HIV patients: epidemiology, mechanisms, and management. Endocrine *41*, 1–10. https://doi.org/10.1007/s12020-011-9565-z.

56. Kalra, S., Kalra, B., Agrawal, N., and Unnikrishnan, A. (2011). Understanding diabetes in patients with HIV/AIDS. Diabetol. Metab. Syndr. *3*, 2. https://doi.org/10.1186/1758-5996-3-2.

57. Non, L.R., Escota, G.V., and Powderly, W.G. (2017). HIV and its relationship to insulin resistance and lipid abnormalities. Transl. Res. *183*, 41–56. https://doi.org/10.1016/j.trsl.2016.12.007.

58. Khuder, S.S., Chen, S., Letendre, S., Marcotte, T., Grant, I., Franklin, D., Rubin, L.H., Margolick, J.B., Jacobson, L.P., Sacktor, N., et al. (2019). Impaired insulin sensitivity is associated with worsening cognition in HIV-infected patients. Neurology *92*, e1344–e1353. https://doi.org/10.1212/WNL.0000000000007125.

59. Gralle, M. (2017). The neuronal insulin receptor in its environment. J. Neurochem. *140*, 359–367. https://doi.org/10.1111/jnc.13909.

60. Holscher, C., and Li, L. (2010). New roles for insulin-like hormones in neuronal signalling and protection: new hopes for novel treatments of

Alzheimer's disease? Neurobiol. Aging *31*, 1495–1502. https://doi.org/10.1016/j.neurobiolaging.2008.08.023.

61. De Felice, F.G., Vieira, M.N.N., Bomfim, T.R., Decker, H., Velasco, P.T., Lambert, M.P., Viola, K.L., Zhao, W.Q., Ferreira, S.T., and Klein, W.L. (2009). Protection of synapses against Alzheimer's-linked toxins: insulin signaling prevents the pathogenic binding of Abeta oligomers. Proc. Natl. Acad. Sci. USA *106*, 1971–1976. https://doi.org/10.1073/pnas.0809158106.
62. McNay, E.C., Ong, C.T., McCrimmon, R.J., Cresswell, J., Bogan, J.S., and Sherwin, R.S. (2010). Hippocampal memory processes are modulated by insulin and high-fat-induced insulin resistance. Neurobiol. Learn. Mem. *93*, 546–553. https://doi.org/10.1016/j.nlm.2010.02.002.
63. Longo, V.D. (2009). Linking sirtuins, IGF-I signaling, and starvation. Exp. Gerontol. *44*, 70–74. https://doi.org/10.1016/j.exger.2008.06.005.
64. Liang, F., Kume, S., and Koya, D. (2009). SIRT1 and insulin resistance. Nat. Rev. Endocrinol. *5*, 367–373. https://doi.org/10.1038/nrendo.2009.101.
65. Lu, M., Sarruf, D.A., Li, P., Osborn, O., Sanchez-Alavez, M., Talukdar, S., Chen, A., Bandyopadhyay, G., Xu, J., Morinaga, H., et al. (2013). Neuronal Sirt1 deficiency increases insulin sensitivity in both brain and peripheral tissues. J. Biol. Chem. *288*, 10722–10735. https://doi.org/10.1074/jbc.M112.443606.
66. He, Y., Hsuchou, H., Wu, X., Kastin, A.J., Khan, R.S., Pistell, P.J., Wang, W.H., Feng, J., Li, Z., Guo, X., and Pan, W. (2010). Interleukin-15 receptor is essential to facilitate GABA transmission and hippocampal-dependent memory. J. Neurosci. *30*, 4725–4734. https://doi.org/10.1523/JNEUROSCI.6160-09.2010.
67. Lonze, B.E., and Ginty, D.D. (2002). Function and regulation of CREB family transcription factors in the nervous system. Neuron *35*, 605–623. https://doi.org/10.1016/s0896-6273(02)00828-0.
68. Suzuki, A., Stern, S.A., Bozdagi, O., Huntley, G.W., Walker, R.H., Magistretti, P.J., and Alberini, C.M. (2011). Astrocyte-neuron lactate transport is required for long-term memory formation. Cell *144*, 810–823. https://doi.org/10.1016/j.cell.2011.02.018.
69. Newman, L.A., Korol, D.L., and Gold, P.E. (2011). Lactate produced by glycogenolysis in astrocytes regulates memory processing. PLoS One *6*, e28427. https://doi.org/10.1371/journal.pone.0028427.
70. Eraso-Pichot, A., Brasó-Vives, M., Golbano, A., Menacho, C., Claro, E., Galea, E., and Masgrau, R. (2018). GSEA of mouse and human mitochondriomes reveals fatty acid oxidation in astrocytes. Glia *66*, 1724–1735. https://doi.org/10.1002/glia.23330.
71. Belanger, M., Allaman, I., and Magistretti, P.J. (2011). Brain energy metabolism: focus on astrocyte-neuron metabolic cooperation. Cell Metab. *14*, 724–738. https://doi.org/10.1016/j.cmet.2011.08.016.
72. Taib, B., Bouyakdan, K., Hryhorczuk, C., Rodaros, D., Fulton, S., and Alquier, T. (2013). Glucose regulates hypothalamic long-chain fatty acid metabolism via AMP-activated kinase (AMPK) in neurons and astrocytes. J. Biol. Chem. *288*, 37216–37229. https://doi.org/10.1074/jbc.M113.506238.
73. Staricha, K., Meyers, N., Garvin, J., Liu, Q., Rarick, K., Harder, D., and Cohen, S. (2020). Effect of high glucose condition on glucose metabolism in primary astrocytes. Brain Res. *1732*, 146702. https://doi.org/10.1016/j.brainres.2020.146702.
74. Yoo, S.-W., Agarwal, A., Smith, M.D., Khuder, S.S., Baxi, E.G., Thomas, A.G., Rojas, C., Moniruzzaman, M., Slusher, B.S., Bergles, D.E., et al. (2020). Inhibition of neutral sphingomyelinase 2 promotes remyelination. Sci. Adv. *6*, eaba5210. https://doi.org/10.1126/sciadv.aba5210.
75. Haughey, N.J., and Mattson, M.P. (2003). Alzheimer's amyloid beta-peptide enhances ATP/gap junction-mediated calcium-wave propagation in astrocytes. NeuroMolecular Med. *3*, 173–180.
76. Knobloch, M., Pilz, G.A., Ghesquière, B., Kovacs, W.J., Wegleiter, T., Moore, D.L., Hruzova, M., Zamboni, N., Carmeliet, P., and Jessberger, S. (2017). A Fatty Acid Oxidation-Dependent Metabolic Shift Regulates Adult Neural Stem Cell Activity. Cell Rep. *20*, 2144–2155. https://doi.org/10.1016/j.celrep.2017.08.029.
77. Pham, L., Komalavilas, P., Eddie, A.M., Thayer, T.E., Greenwood, D.L., Liu, K.H., Patterson, A., Fessel, J.P., Boyd, K.L., et al. (2022). Neutrophil trafficking to the site of infection requires Cpt1a-dependent fatty acid β-oxidation. Commun. Biol. *5*, 1366.
78. Trabjerg, M.S., Andersen, D.C., Huntjens, P., Mørk, K., Warming, N., Kullab, U.B., Skjønnemand, M.L.N., Oklinski, M.K., Oklinski, K.E., Bolther, L., et al. (2023). Inhibition of carnitine palmitoyl-transferase 1 is a potential target in a mouse model of Parkinson's disease. NPJ Parkinsons Dis. *9*, 6.
79. Kramer, A., Green, J., Pollard, J., Jr., and Tugendreich, S. (2014). Causal analysis approaches in Ingenuity Pathway Analysis. Bioinformatics *30*, 523–530. https://doi.org/10.1093/bioinformatics/btt703.
80. Chong, J., Wishart, D.S., and Xia, J. (2019). Using MetaboAnalyst 4.0 for Comprehensive and Integrative Metabolomics Data Analysis. Curr. Protoc. Bioinformatics *68*, e86. https://doi.org/10.1002/cpbi.86.

STAR★METHODS

KEY RESOURCES TABLE

REAGENT or RESOURCE	SOURCE	IDENTIFIER
Antibodies		
Insulin receptor	Cell Signaling Technology	3035S; RRID: AB_2924796
GFAP	Millipore Sigma	G3893; RRID: AB_477010
C57BL/6J	Jackson Laboratory	000664
(GFAP)-Cre ERT2 mice	Jackson Laboratory	012849
(IR)-floxed mice	Jackson Laboratory	006955
Chemicals, peptides and recombinant proteins		
Insulin	Millipore Sigma	91077C
Etomoxir	Millipore Sigma	E109S
Glutamic acid-D3	Cambridge Isotope Laboratories, Inc	DLM-335-1
Citric acid-D4	Cambridge Isotope Laboratories, Inc	DLM-3487-0.5
Butyryl-L-carnitine	Cayman Chemicals	26542
Lauroyl-/-carnitine-D3	Cayman Chemicals	26571
Cytosine-D2	CDN isotopes	D6872
Tyrosine-D2	Cambridge Isotope Laboratories, Inc	DLM-2317-0.5
L-tryptophan D5	Cayman Chemicals	34829
Caffeine-13C2	Toronto Research Chemicals	C080101
L-leucenol	Cayman Chemicals	14337
Sulfinpyrazone	Cayman Chemicals	17847
$^{13}C_{16}$ palmitate	Toronto Research Chemicals	P144505
Oil Red O	Millipore Sigma	O0625
Software and algorithms		
Tophat	TOP HAT	2.0
Bowtie	Bowtie	1.1
Partek Genomics Suite	Parteck Inc	V6.6
Ingenuity Pathways Analysis	QIAGEN	
MetaboAnalyst	taboAnalyst	5.0
Sciex accurate MS/MS spectral library	Sciex	2.0
MultiQuant	Sciex	1.3
Zeiss Axio Imager	Zeiss	A1
Applied Biosystem 7300	Life Technology	
LTP analysis software	MATLAB 2020A	https://haugheylab.org/

EXPERIMENTAL MODEL AND STUDY PARTICIPANT DETAILS

Mice

Male C57B1/6J mice 3–4 months of age were obtained from the Jackson Laboratory (Bar Harbor, ME, USA). Mice were single-housed in a temperature and humidity-controlled room under a 12 h light cycle with food and water available *ad libitum.* All animal procedures were approved by the Johns Hopkins University Animal Care and Use Commit. Mice with a conditional knock out of the insulin receptor were previously created using the Cre-loxP system. Male astrocytic glial fibrillary acidic protein (GFAP)-Cre ERT2 mice (Jax 012849) were crossed with female insulin receptor (IR)-floxed mice (Jax 006955). GFAP-IR mice were crossed to achieve hemizygous GFAP-Cre and homozygous IR. Recombination of floxed IR was induced by intraperitoneal injection of 4-hydroxytamoxifen for 5-consecutive days at 3–4 weeks of age.[74] Mice were used for experimentation at 3–4 months of age.

Astrocyte culture

Rat primary astrocyte cultures were prepared as previously described.[75] In brief, the cerebral cortex of postnatal day 1 Sprague-Dawley rats Cortices were isolated in a Hanks' balanced salt solution (Corning, Manassas, VA) containing Dulbeccos's modified Eagle's medium/F-12 media (Gibco BRL) supplemented with 10% fetal bovine serum (Gibco BRL), D-glucose (final concentration 25 mM) (Sigma), and 1% antibiotic/antimitotic solution (104 Unit of penicillin G/ml, 10 mg streptomycein/ml and 25 μg amphotericin B/ml) (Sigma). Cells were plated in DMEM/F12 (Gibco, Grand Island, NY), containing D-glucose (7.5 mM. Sigma, St. Louis, MO), 10% FBS (Sigma, St. Louis, MO), and antibiotic/antimycotic mix (10,000 units/mL of penicillin, 10,000 μg/mL of streptomycin, and 25 μg/mL of Fungizone Antimycotic, Gibco, Grand Island, NY) in a T-75 culture flask, coated with poly-D-lysine hydrobromide (Sigma, Saint Louis, MO). Culture flasks were secured to a rotary shaker (Thermo Scientific) and shaken at 200 rpm in a tissue culture incubator (Thermo Scientific) for 18 h at 37′C in 5% CO_2 environment. Less adherent cells were removed with the media and fresh media was added to the cells. Cells were incubated at 37°C and 5% CO_2 with complete media changes every 2–3 days. One week following isolation, type 1 astrocytes were purified by orbital shaking at 200 rpm for 8 h in an incubator maintained at 37°C and 5% CO_2. Loosely adherent cells were discarded, and adherent astrocytes were 98% GFAP+ astrocytes with type I morphology. Astrocytes were used for experiments between 3 and 4 passages.

METHOD DETAILS

RNA sequencing

Male C57B1/6J (12 weeks) or GFAP-IR KO mice were treated with 5 μL of saline or insulin (2.4 IU) per nare at time points 0, 15 min, 6 h and 12 h ($N = 3$). At the end of each time point, mice were anesthetized using isoflurane, brains were extracted, and hippocampus tissue was isolated. Tissues were flash frozen in liquid nitrogen, then stored in −80′C. Astrocytes were seeded at 5×10^4 cells per well on 6-well plates coated with PDL in DMEM/F12 (Gibco BRL) supplemented with 10% FBS, D-glucose (final concentration 25 mM) (Sigma), and 1% antibiotic/antimitotic solution (104 Unit of penicillin G/ml, 10 mg streptomycin/ml and 25 μg amphotericin B/ml) (Sigma). Four hours before treatment, media was changed to DMEM/F12 (Gibco BRL) supplemented with 2% FBS, D-glucose (final concentration 5 mM) (Sigma), and 1% antibiotic/antimitotic solution (104 Unit of penicillin G/ml, 10 mg streptomycin/ml and 25 μg amphotericin B/ml) (Sigma). Astrocytes were treated with saline or 200 nM insulin (Sigma) at time points 6 and 12 h. Hippocampal neurons seeded at 8×10^5/well in 6-well plates coated with PEI and in serum free Neurobasal medium containing 1% B27. At 14 days DIV, and 4 h before treatment, media was changed to serum free Neurobasal medium containing 1% B27 (insulin-free). Hippocampal neurons were treated with saline or 200 nM insulin (Sigma) at 0, 6 or 12 h. After each timepoint, astrocytes and hippocampal neurons were collected in RLT buffer containing 2-Mercaptoethanol, and processed using the RNeasy Mini Kit (Qiagen, Venlo, Limburg), and stored at −80°C. Sequencing (Illumina 1.9, San Diego, CA) was conducted by the Johns Hopkins Deep Sequencing and Microarray Core Facility. Briefly, each of the biological sample's raw pair-end reads were aligned to NCBI's mouse sequence (hippocampal tissue) or NCBI's rat sequence (astrocytes and hippocampal neurons) build RGSC_v3.4 with the TopHat read mapping and transcriptome alignment platform (Tophat 2.0 and Bowtie 1.1). Analyses were performed with the Partek Genomics Suite v6.6 platform (Partek Inc. St Louis MO, USA). Reads per kilobase of transcript per million mapped reads (Rpkm) were calculated and used to convert the data to log2 notation (with zero values being assigned arbitrary an 0.001). Data was then quantile normalized in order to minimize technical inter-sample variation. The resulting normalized values were compared between experimental time points by 1-way ANOVA to determine fold change and p-values for each of the approximately 16.9 K annotated transcripts. Transcripts with low expression values (<4 hits per gene) and low fold change (<2 standard deviations from control) were excluded from Gene Ontology (GO) analysis.

Cell and tissue processing for fatty acid detection by mass spectrometry

Astrocytes were seeded at 5×10^4 cells per well on 6-well plates coated with PDL in DMEM/F12 (Gibco BRL) supplemented with 10% FBS, D-glucose (final concentration 25 mM) (Sigma), and 1% antibiotic/antimitotic solution (104 Unit of penicillin G/ml, 10 mg streptomycin/ml and 25 μg amphotericin B/ml) (Sigma). Four hours before treatment, media was changed to DMEM/F12 (Gibco BRL) supplemented with 2% FBS, D-glucose (final concentration 5 mM) (Sigma), and 1% antibiotic/antimitotic solution (104 Unit of penicillin G/ml, 10 mg streptomycin/ml and 25 μg amphotericin B/ml) (Sigma). Astrocytes were treated with either no treatment, 200 nM insulin (Sigma) or 10 μM of CPT1 inhibitor, etomoxir (Millipore) at 0, 1, 3, 6 and 12h. Hippocampal neurons were seeded at 8×10^5 cells/well in 6-well plates coated with PEI and in serum free Neurobasal medium containing 1% B27. At 14 days DIV, and 4 h before treatment, media was changed to serum free Neurobasal medium containing 1% B27 (insulin-free). Cells were treated with 200 nM insulin (Sigma) or no treatment at 0, 1, 3, 6 and 12 h. Cells were collected in water and centrifuged at 13,000 rpm for 30 min. Supernatant was discarded and cell pellet was stored −80′C until ready for processing by mass spectrometry.

Male C57B1/6J (12 weeks) were treated with 5 μL of saline, insulin (2.4 IU) or with CPT1 inhibitor (0.16μg/nair; 0.322μg/total; Millipore) per nare at time points 0, 1, 3, 6 and 12 h. After each treatment, mice were anesthetized with isoflurane, perfused with saline, brains were isolated and flash frozen in liquid nitrogen and stored in −80′C before processing for mass spectrometry.

Liquid chromatography-quadrupole time of Flight mass spectrometry for untargeted metabolomics analysis

Chemicals and materials

Fatty acid standards were purchased from Sigma-Aldrich (Sigma-Aldrich, Milan, Italy), Matreya LLC Lipids and Biochemicals (PA, USA) and Cayman Chemicals (Ann Arbor, Michigan 48108 USA). Deuterium labeled internal standards including: Glucose-D7, Glucose-6-phosphate-13C6, Octanoic acid-D15, Lauric acid-D23, Citric acid-D4 were purchased from Cambridge isotopes ltd (Tewksbury, MA, USA), butyryl-L-carnitine (chloride) and Lauroyl-/-carnitine-D3-(chloride) were from Cayman chemicals (Ann Arbor, MI, USA). HPLC-grade Methanol and Chloroform were purchased from Honeywell International Inc. (Morristown, NJ, USA). Ammonium Formate from Sigma-Aldrich and Silical Gel (SiOH) cartridges used for solid phase extraction were from Agilent Technologies (Folscom, CA, USA). Deionized water obtained using Milli-Q system (Millipore, Vimodrone, Milan, Italy).

Extraction of metabolites

Cell samples (protein normalized) were vigorously homogenized using extraction solvent, 70% ice-cold methanol (0.5% 1N HCl), pre-spiked with 12 isotopically labeled internal standards that included: glucose-D7, glucose-6-phosphate-13C6, octanoic acid-D15, lauric acid-D23, glutamic acid-D3, citric acid-D4, butyryl-L-carnitine, lauroyl-/-carnitine-D3-(chloride), cytosine-D2, Tyrosine-D2, L-tryptophan D5 and caffeine-13C2 for 5 min using a TissueLyser LT (Qiagen, Switzerland) at 50Hz, and centrifuged at 13000 rpm at 4C for 20 min using. The supernatants containing internal standards and unknown metabolites were collected and evaporated to complete dryness using a vacuum concentrator (Thermo Scientific ''Savant SpeedVac'' SPD 120P2, Waltham, MA, USA). The residues were then resuspended in 150 μL of 50% ice-cold methanol containing 0.1% formic acid and two additional standards, L-leucenol and sulfinpyrazone (2 ppm each) that were used to track instrument performance and mass accuracy throughout the analyses. Samples were vortexed, centrifuged at 13000 rpm at 4°C for 10 min, and supernatants collected for metabolomics profiling.

UFLC-QTOF-HRMS/MS analysis

Metabolomic profiling was performed using an ultrafast liquid chromatography (Shimadzu, Kyoto, Japan) coupled to a TripleTOF 5600 (AB Sciex, Concord, CA, USA) high resolution mass spectrometer (UFLC-HRMS/MS). The UFLC system consisted of a degasser, a quaternary pump, an autosampler, and a temperature-controlled column compartment. The TripleTOF 5600 mass spectrometer was equipped with DuoSpray Turbo V-dual ESI/APCI source probes. The mass spectrometer used an automated calibrant delivery system that was delivered every 15 sample injections by manufacturer recommended calibrants to maintain the mass accuracy of the instrument below 5 ppm. Ten microliters of each extracted sample were subjected to UFLC-HRMS/MS analysis for metabolomic profiling. Metabolites were chromatographically separated on a Kinetex Pentafluorophenyl (PFP/F5) stationary phase (Phenomenex, Torrance, CA, USA) using a binary gradient mobile phase program (acetonitrile-eluent A and ddH2O-eluent B; both contained 0.1% FA) with the following parameters: 0–3 min 100% eluent B, 3–13 min, eluent A increased from 0% to 100%, 13–19 min eluent A hold at 100%, 19–19.10 eluent B increased to 100% from 0%, and hold for 4 min to allow for column equilibration before the next sample is introduced into the system. The UFLC-separated metabolites were introduced into electrospray ionization chamber for data acquisition in both positive and negative modes over a mass range of 30–900 m/z. Data were acquired and collected in an Information Dependent Acquisition (IDA-HRMS/MS) metabolomics approach, which attains accurate m/z (mass to charge ratio) of both the pre-cursor and fragments of each metabolite in the samples within a given mass range i.e., 30–900 m/z. The acquired data were processed using Sciex OS -Q1.5 data analysis software (AB SCIEX, Concord, Canada) integrated with the NIST (2017) tandem mass spectral library, and the Sciex accurate MS/MS spectral library 2.0 for peak detection, peak alignment, spectral processing, feature identification based on matching pairs of precursor-fragment ions to the tandem MS databases, and peak quantification. Pooled cell sample homogenates (all experimental samples) were extracted and analyzed in untargeted mass spectrometric workflow to generate a reliable and reproducible targeted list of metabolites. Metabolite extracted pooled samples were analyzed in eight sequential injections using our LC-HRMS/MS system as described above. In order to be included in the targeted list, any given metabolite must be apparent in 7 of 8 analytical runs with a coefficient of variation (CV) less than 20%. The metabolites meeting these criteria were used to create a targeted list that was used to identify these pre-validated metabolites in experimental samples.

Quadrupole ion trap mass spectrometry for targeted analysis

Chromatographic conditions

Chromatographic experiments were carried out on a Shimadzu Prominence HPLC system (Shimadzu, Columbia, MD, USA) consisted of an autosampler, column compartment, degasser and Pumps. Octadecylsilane, C_{18} (2.6μm, 50 × 2.1mm) (Phenomenex, Torrance, CA, USA) was used for the separation of fatty acids and maintained at 55°C. The autosampler (Shimadzu SIL-20AC) was maintained at 15°C and ten μls of each sample solution was injected for the analysis. A binary gradient mobile phase program was optimized for the separation of fatty acids. Mobile phase-B consisted of methanol containing 10 mM ammonium formate and mobile phase-A consisted of methanol: water (37:63, v/v) containing 10mM ammonium formate. The initial B concentration was kept at 30%. A linear gradient was used as follows: 0.1 min 30%B; 4.0 min 100%B; 8 min 100%B; 9 min 30%B; 10 min stop, at a flow rate of 0.4 mL/min. The total run time for each sample run was 10 min.

Mass spectrometric conditions

Tandem mass spectrometric (MS/MS) analysis were performed on a quadrupole ion trap mass spectrometer (API 4000- Q TRAP, Applied Biosystems, Foster City, CA, USA)- equipped with a Turbo Ion Spray (TIS) source. The data were acquired (using Analyst version 1.5.1) in negative electrospray ionization for fatty acids, glucose, pyruvate, lactate, TCA cycle products, and

β-hydroxybutyrate, and positive electrospray ionization for fatty acylcarnitines. All the analytes were detected in pseudo multiple reaction monitoring (MRM) mode, and the data were processed and quantified using MultiQuant 1.3.

Metabolic flux experiment using $^{13}C_{16}$ palmitate

Astrocytes or neurons incubated with the corresponding medium containing 50μM ^{13}C-ubiquitousley isotopic labeled palmitate ($^{13}C_{16}$ palmitate -Toronto Research Chemicals, Canada) with or without INS exposure or etomoxir (10 μM), CPT1 inhibitor at 3, 6, and 12h separately. $^{13}C_{16}$ _palmitate was coupled to BSA prior adding to cells to attain enhanced cellular uptake as described earlier.[76] Metabolites were extracted from cell lysate with 1 mL of 50% ice-cold methanol containing Citrate-D4 internal standard, centrifuged, and the extracts were dried using a vacuum centrifuge (SPD120, ThermoFisher, USA). The dried fractions were resuspended in 100 μL of 50% methanol containing 0.1% formic acid. The cellular uptake of $^{13}C_{16}$ palimitate and its carnitine conjugate ($^{13}C_{16}$-palmitoyl-carnitine), and enrichment of ^{13}C-atoms of resultant [2-^{13}C] acetyl-CoA into TCA cycle intermediates were measured in targeted multiple reaction monitoring mode using ion trap mass spectrometer.

Quantitative Real-Time PCR

Astrocytes were seeded at 5 × 10^4 cells/well in 6-well plates and treated with 200 nM insulin or no treatment for 0, 1, 6 and 12 h. Cells were collected in RLT buffer containing 2-Mercaptoethanol, processed using the RNeasy Mini Kit (Qiagen, Venlo, Limburg), and stored at −80′ C until reverse transcription. RNA (1 μg) was brought to a final volume of 10 μL with DEPC H_2O containing Random Primers (1 μL; Invitrogen, Carlsbad, CA) and dNTP's (1 μL of 10 mM stock; Promega, Madison, WI). Samples were incubated at 65°C for 5 min then put on ice. A master mix containing 5× first strand buffer (4 μL; Invitrogen, Carlsbad, CA), DTT (2 μL of 0.1 M; Invitrogen, Carlsbad, CA), RNase inhibitor (1μL; Thermofisher, Waltham, MA) and Superscript II RT (1 μL; Invitrogen, Carlsbad, CA) was made and a final volume of 8 μL was added to each reaction. Samples were incubated at room temperature for 10 min, 42°C for 50 min, then 70°C for 15 min cDNA was stored at −20°C. For quantitative real-time PCR (qRT-PCR), each reaction contained DEPC H20 (10.5 μL), SYBR Green Master Mix (12.5 μL; Life Technology, Carlsbad, CA), forward primer (0.5 μL; Sigma, St. Louis, MO), reverse primer (0.5 μL; Sigma, St. Louis, MO), and cDNA (1 μL). Primer specific concentrations were individually optimized for each gene to produce a single PCR product with no primer-dimer formation. Each 96 well plate included a non-template control, and each sample was analyzed in triplicate on an Applied Biosystem 7300 (Life Technology, Carlsbad, CA). Cycling parameters were as follows: 1 cycle at 50°C for 2 min, 1 cycle at 95°C for 10 min, 40 cycles of 95°C for 15 s, and 60°C for 1 min. The dissociation stage was 95°C for 15 s, 60°C for 1 min and 95°C for 15 s. The change in threshold cycle (ΔΔΔCt) for each sample was normalized to β-actin. ΔΔΔCt's were calculated by comparing ΔΔΔCt for the treatment group to the average ΔΔΔCt of the control group. qRT-PCR data was analyzed by logarithmically raising the changes in ΔΔΔCt the values, 2^{-}ΔΔΔCt ^{Ct} and expressed as a fold change.

Oil Red O staining

Astrocytes were seeded at 2 × 10^4 cells/well in DMEM/F12 (Gibco BRL) supplemented with 10% FBS, D-glucose (final concentration 25 mM) (Sigma), and 1% antibiotic/antimitotic solution (104 Unit of penicillin G/ml, 10 mg streptomycin/ml and 25 μg amphotericin B/ml) (Sigma) on PDL coated glass coverslips. When cells reached 70% confluency, media was changed to DMEM/F12 supplemented with 2% FBS and 5 mM D-glucose for 4 h before treatment. Astrocytes were treated with saline or 200 nM insulin (Sigma) for 1, 1.5, 3, 6 and 24 h. At the end of each time point, cells were washed with 1× PBS twice. Cells were then fixed by incubating in 4% paraformaldehyde (PFA) for 15 min at RT. Cells were then washed with 1× PBS twice. Freshly prepared 5% Oil Red O (Sigma) was added to the cells and incubated at RT for 60 min. Stain was then removed, and cells were washed with PBS 1-3 x's. Cells were then counterstained with Mayer's hematoxylin (Thermo Fisher Scientific). Image analysis was performed using a Zeiss Axio Imager.A1 at 40×.

Measurement of fatty acid and glucose uptake

The uptake of fatty acids was studied using a free fatty acid uptake fluorometric kit (Abcam Cambridge, Massachusetts) according to the manufacturer's guidelines. Astrocytes were seeded at 2 ^{x} 10^3 cells/well in a 96-well plate overnight in DMEM: F12 media containing 10% FBS. After 16–18 h media was changed to low FBS containing media for 1 h. Hippocampal neurons were plated at a density of 4 × 10^4 cells/ml in a 96-well plate in neurobasal media containing 1% B27. The next day, media was changed to neurobasal media containing 1% B27-insulin free (Invitrogen). Cells were then treated with 200 nm Insulin and the plate was read at the end of each timepoint. Fluorescence signal was measures with a fluorescence microplate reader at excitation wavelength 485 nm and an emission wavelength of 515 nm. FA uptake was calculated by the fluorescence readings in the blank wells subtracted from the values for the wells containing cells and treatment.

Glucose uptake activity was measured using a glucose uptake assay (Cayman Chemical Ann Arbor, MI), following the product protocol. Briefly, astrocytes were seeded at 2 ^{x} 10^3 cells/well in a 96-well plate and incubated in DMEM: F12 media containing 10% FBS overnight. Hippocampal neurons were plates at a density of 4 × 10^4 cells/ml in a 96-well plate in neurobasal media containing 1% B27. The next day, media was changed to neurobasal media containing 1% B27-insulin free (Invitrogen). Cells were washed with PBS and treated with 200 nm insulin in low FBS and glucose free media containing 100ug/ml of fluorescent D-glucose analogue 2-[N-(7-nitrobenz-2oxa-1,3,diazol-4-yl)amino]-2-deoxy-D-glucose (2-NBDG) for 5, 10, 15, 20 and 30 min time points. At the end of the treatment, the supernatant was aspirated and 200 μl of cell-based assay buffer was added to each well. The supernatant was then

aspirated again and 100 μl of cell-based assay buffer was added to each well. Fluorescence was measured at an excitation wavelength of 485 nm and an emission wavelength of 535 nm.

Mitochondrial stress test

Astrocytes were seeded at 1 × 10^3 in a clear bottom 96-well plate (Agilent Seahorse XF Cell Culture Microplate) coated with PDL in DMEM/F12 (Gibco BRL) supplemented with 10% FBS, D-glucose (final concentration 25 mM) (Sigma), and 1% antibiotic/antimitotic solution (104 Unit of penicillin G/ml, 10 mg streptomycin/ml and 25 μg amphotericin B/ml) (Sigma). When cells reach confluency, media was changed to DMEM/F12 supplemented with 2% FBS and 5 mM D-glucose for 4 h before treatment. Hippocampal neurons were plates at a density of 4 × 10^4 cells/ml in a 96-well plate (Agilent Seahorse XF Cell Culture Microplate) coated with Neurobasal medium containing 1% B27. At 14 days DIV, and before treatment, media was changed to serum free Neurobasal medium containing 1% B27 (insulin-free). Cells were treated with either 200 nM insulin only for 30 or 60 min, fatty acid mixture only (2% stearic acid, 3% oleic acid and 8% DHA and EPA conjugated to 0.5% BSA) for 30 or 60 min and insulin plus fatty acid mixture for 30 or 60 min. After each time point, media was removed and the mitochondrial stress test (Agilent) was performed according to manufacturer's instructions.

Long-term potentiation

Electrophysiological experiments were performed on hippocampal slices from 12 week-old C57/BL6 mice. Coronal brain slices containing central part of hippocampus (300μm thick) were sectioned using a Leica VT 1200 vibratome in ice-cold ACSF containing (in mM): 128 NaCl, 3 KCl, 26 $NaHCO_3$, 1 NaH_2PO_4, 0.6 $MgSO_4$, 10 glucose and 2 $CaCl_2$ and saturated with 95% O_2 and 5% CO_2. Brain slices were incubated for at least 1 h at room temperature (22°C–24°C) in a holding chamber filled with ACSF prior to use.

Animal treatments for LTP

Intranasal insulin was delivered at each nare (INI; 2.4 IU/nare, 4.8 IU total) and corresponding similar volume of saline was delivered as a control. Etomoxir was delivered intranasally for CPT-1 inhibition at 100 uM concentration[77,78] (0.16μg/nair; 0.322μg/total) 1 h before administration of insulin/saline. Animals were tested after 6 h post insulin/saline administration. For the insulin receptor knockdown experiments, adeno-associated virus harboring shRNA sequences against insulin receptor (5′-GCATGGATATCCGGAACAACC-3′) or a nontargeting shRNA (5′-GGGTGAACTCACGTCAGAA-3′) were cloned into the AAV(DJ/8)-GFAP-GFP-shRNA backbone vector (SignaGen Laboratories, Rockville, MD, USA). Adult male C57BL6 mice (2-3-month-old) were anesthetized with 3% isofluorane (Baxter, Deerfield, IL, USA) in oxygen (Airgas, Radnor, PA, USA), and placed in stereotactic frame (Stoelting Co, Wood Dale, IL, USA). A small burr hoe was drilled in the skull over the left hippocampal CA1 area using a dental drill (Fine Scientific Tools, Foster City, CA, USA). AAV(DJ/8)-GFAP-GFP-$shRNA_{InsR}$ or AAV(DJ/8)-GFAP-GFP-$shRNA_{scr}$ was injected (total volume of 0.5 μL) into the pyramidal neurons of CA1 in hippocampus at the rate of 0.5 μL/min via a pulled glass capillary tip diameter <50 μm. Stereotactic coordinates were AP, −2.0; ML, +2.0; DV, +1.5. The mice were allowed to recuperate for 48 h and evaluated LTP following 6 h of INI administration.

Multichannel Systems MEA2100-Lite was used to perform all electrophysiological experiments. Hippocampal slices were placed on an 8 × 8 3D multielectrode array (MEA) submerged in artificial cerebrospinal fluid (ACSF) bath. The MEA plate and the bath were grounded via an Ag/AgCl pellet attached to the MEA amplifier ground socket. Brain slices were positioned and immobilized using a silver ring with nylon mesh (Warner Instruments, IRC 41 × 1 × 1.5mm), and position images using a Zeiss inverted microscope. ACSF (∼37C) was perfused by peristaltic pump system (PPS2, Multichannel Systems) bubbled with 95% O_2 and 5% CO_2 delivered at a flow rate of 1.5–2.0 mL/min through a temperature controlled (TC02, Multichannel Systems) perfusion cannula (PH01, multichannel systems). Monopolar stimulation was delivered to the Shaffer collateral/commissural fibers near the CA1/CA3 border. Biphasic voltage pulses (positive/negative, 100 μs/phase) were delivered to the stimulation electrodes. I/O relationships were obtained, and baseline stimulus strength was set at an intensity sufficient to elicit 30–40% of maximal field excitatory potentials (fEPSPs). After establishing a stable baseline for 20 min LTP was induced by applying 2 trains of theta burst stimulation (TBS) spaced 2 min apart at 1.5 times the baseline intensity. Each TBS train consisted of 10 bursts of high frequency stimulus (each burst consisted of 4 pulses at 100 Hz) delivered with an inter burst interval of 170 ms. Activity was recorded for 60 min after induction of LTP. The column of electrodes that run perpendicular to the SR in the pyramidal cell layer of CA1 were used for analysis. A normal distance between recording and stimulating electrodes was maintained at 100-200 μm. Evoked fEPSP responses were filtered by bandpass filter design in MATLAB and average amplitudes of fEPSP (A five point averaging was done over the dataset) were used for analysis. Normalized responses of the recording electrodes were compared before and after LTP induction. All analysis was performed in MATLAB 2020a. Potentiation was quantified and statistical analysis was performed for 1 min and 60 min following the induction of LTP by TBS. Spectral analysis of the potentiated electrophysiological signals 1 min after induction of LTP was performed using continuous wavelet transformation in MATLAB to check for time-frequency information in the fEPSP potentiated responses that could suggest for additional synaptic inputs during treatment conditions (which in this case may be lactate during treatment with insulin).

Primary neuronal culture

Primary hippocampal neuronal cultures were prepared from embryonic day 18 Sprague-Dawley rats as described previously (Haughey Alzheimer's amyloid-beta peptide enhances 2003). Briefly, hippocampal tissues were dissected from isolated cortices in Hanks' Balanced Salt Solution (Corning, Manassas, VA; calcium, magnesium and phenol red free). Tissues were enzymatically

and mechanically dissociated with trypsin and trituration into a single cell suspension. Hippocampal neurons resuspended in Neurobasal media (Gibco) containing B27 supplement (Gibco), 1% antibiotic/antimitotic solution (104 Unit of penicillin, 10 mg streptomycin/ml and 25 μg amphotericin B/ml) (Sigma), 5% FBS (Sigma, St. Louis, MO), HEPES (4.8 mM, Sigma, St. Louis, MO) and L-glutamine (1.2 mM, Sigma, St. Louis, MO) and plated with polyethyleneimine (PEI, Sigma, St. Louis, MO) coated culture dishes. Three hours after plating, media was replaced with serum free Neurobasal medium containing 1% B27 and supplemented every 7 days. Hippocampal neurons were used at 14 DIV for experiments.

QUANTITATION AND STATISTICAL ANALYSIS

Statistical analysis

Statistical comparisons were performed using GraphPad Prism version 10. Unpaired Student's t-tests were used to determine experimental differences between two groups. A one-way ANOVA was used to compare experimental differences between three or more groups, followed by Tukey's post-hoc test to identify specific pairwise differences. Data normality was assessed using the Shapiro-Wilk test prior to parametric analyses, and non-normally distributed data were analyzed using the Mann-Whitney U test for two groups or Kruskal-Wallis test with Dunn's post-hoc test for multiple groups. Significance was considered at $p < 0.05$.

Bioinformatics analysis

RNA sequence pathway analysis and inference of upstream regulators were performed using QIAGEN's Ingenuity Pathways Analysis (IPA; QIAGEN, Redwood City, www.Qiagen.com/ingenuity).[79] Untargeted mass spectrometric data analysis and enriched metabolomics pathway identification were performed using a web based comprehensive metabolomics pipeline Metaboanalyst 5.0.[80] Metabolite identification required matching the precursor ion and more than 70% of its fragment ions to a particular metabolite. Targeted metabolomics list was generated by analyzing the pooled samples in octuplicate. In order to be considered for metabolites in the final targeted list, those pass the following conditions: 1. the metabolite should present in more than 6 analyses, 2. the coefficient of variation (CV) of its ''are under the curve'' (AUC) should be less than 20% in all the detected analyses. The final targeted list was used to identify the metabolites present in each individual samples. For relative quantification purpose we used peak area under the curve ratios (metabolite/Internal standard) to compare the controls vs. treated groups. Missing metabolites in few samples (less than 30% to the total number of samples) were replaced with the lowest intensity ratio obtained.